Linear-Threshold Network Models for Describing and Analyzing Brain Dynamics

Michael McCreesh[1], Erfan Nozari[2], and Jorge Cortés[1]
1. University of California San Diego, Department of Mechanical and Aerospace Engineering
2. University of California Riverside, Department of Mechanical Engineering

Summary

Over the past two decades, an increasing array of control-theoretic methods have been used to study the brain as a complex dynamical system and better understand its structure-function relationship. This article provides an overview on one such family of methods, based on the linear-threshold rate (LTR) dynamics, which arises when modeling the spiking activity of neuronal populations and their impact on each other. LTR dynamics exhibit a wide range of behaviors based on network topologies and inputs, including mono- and multi-stability, limit cycles, and chaos, allowing it to be used to model many complex brain processes involving fast and slow inhibition, multiple time and spatial scales, different types of neural behavior, and higher-order interactions. Here we investigate how the versatility of LTR dynamics paired with concepts and tools from systems and control can provide a computational theory for explaining the dynamical mechanisms enabling different brain processes. Specifically, we illustrate stability and stabilization properties of LTR dynamics and how they are related to goal-driven selective attention, multistability and its relationship with declarative memory, and bifurcations and oscillations and their role in modeling seizure dynamics in epilepsy.

INTRODUCTION

The brain is one of the most complex dynamical systems known to exist. It is composed of billions of interconnected neurons and involved in countless cognitive and physical functions. It has been the holy grail of neuroscience for centuries to explain, at various levels of analysis, how these functions arise from the brain's complex and ever-changing structure. Computational modeling has long been a pillar in this quest for multi-level understanding. Furthermore, the complexity that arises from the interplay between neuronal dynamics, multiple temporal and spatial scales, and the intricate interconnection and rich topological structure observed in the brain makes the use of system-theoretic techniques a natural choice to analyze and understand such computational models. This approach has led to a growing number of recent works at the intersection of control theory and neuroscience, see [1], [2], [3], [4], [5], [6], [7], [8], [9], [10], [11] for a small sample.

A wide variety of processes and phenomena in the brain have been studied through the use of dynamical systems models.

1066-033X/20©2020IEEE

Visual processing [12], [13], voluntary movement [14], [15], and pathological behavior due to disorders such as Parkinson's or epilepsy [16], [17] are only a few examples. Indeed, the wide range of functions and behaviors exhibited by the brain exceed that of any single model (a brief summary of common models used in neuroscience is given in "Dynamical Systems Models in Neuroscience"). Nevertheless, generalizable, multipurpose models are increasing sought whose dynamics are rich enough to describe multiple dynamical behaviors using a single model structure. In this work we investigate one such model consistent with empirical descriptions of neural physiology, the linear-threshold rate (LTR) dynamics, and illustrate its richness by using it to describe multiple dynamical behaviors observed in the brain. Specifically, we consider the dynamical brain behaviors of goal-driven selective attention (GDSA), declarative memory, and epileptic seizure activity (see "Examples of Neural Activities Through the Lens of Dynamical Systems" for an overview of these applications). Each of these applications can be tackled from a dynamical systems perspective, a choice made due to their dependence on both the structure of the brain and the dynamics occurring within it. For the purpose of fully exploring the rich behavior of the linear-threshold model, the key point is that each of these applications can be associated with distinct dynamical properties, illustrating the versatility of the linear-threshold model.

While these three applications are distinct functions of the brain, there does exist overlap between them. For example, GDSA is a key part of working memory in order to select relevant information from internally stored representations [18], [19]. Meanwhile, epilepsy and memory are tied in that during epileptic seizures the ability of the brain to both encode and retrieve memories is inhibited [20], [21], [22]. As such, while individual models of each dynamical behavior are important, the ability to use a single model that can show all three behaviors is desirable. In this work, through an examination of a dynamical systems approach to GDSA, epileptic seizures, and declarative memory we provide a review of the extensive properties of the linear-threshold dynamics, covering topics such as stability, stabilizability, bifurcations, and oscillations.

Outline

The paper is organized as follows. We first discuss methods of modeling the brain, focusing on firing rate models, leading to the derivation of the linear-threshold model. We also discuss the role of feedback and feedforward control employed in the context of the brain. We then explore properties of the LTR dynamics in single networks through the modeling of selective attention, epilepsy, and memory. We exploit the description of the dynamics as a piecewise-affine state-dependent switched system to leverage system-theoretic tools in unveiling the relationship between the network interconnection structure and its dynamical behavior. This leads to an examination of the construction of interconnected brain networks and study their resulting properties, with a view on the application to selective attention and epilepsy. For selective attention, we consider hierarchical and star-connected interconnected topologies and illustrate the role of feedback/feedforward control in ensuring recruitment of task-relevant regions and inhibition of task-irrelevant regions. For epilepsy, we consider interconnected excitatory-inhibitory pairs and describe conditions for oscillations to emerge and spread throughout the resulting network of networks. We finish with a discussion of additional properties of the dynamics and an outline of additional applications that could be studied using the linear-threshold model.

LINEAR THRESHOLD RATE MODELS

Computational modeling of the brain is particularly challenging due, in part, to the different scales of information in which one can phrase and approach the problem. At the smallest level, or the "microscale", the brain is composed of billions of neurons whose dynamics can be measured at the individual level through their electrical activity. At the opposite end of the spectrum, the "macroscale", the brain can be divided into large regions, each composed of tens of millions of neurons with "activity" patterns recorded using modalities such as functional magnetic resonance imaging (fMRI) or electroencephalography (EEG). Various levels also fall in-between the two extremes, often referred to as the "mesoscale". Each scale is the host to different network structures, elemental components, and connectivity patterns. This heterogeneity of spatial scales alone makes it infeasible to study the brain and all its functions and emerging phenomena using a single computational model.

Both microscale models, illustrating the voltage dynamics of individual neurons, and macroscale models, showing aggregate connectivity between regions, have been the subject of much research using computational models. Details on microscale models can be found in [23], [24], [25], [26] and references therein. For macroscale models, we direct the reader to [27], [28] and references within. Interestingly, while the microscale dynamics at the neuronal level is highly nonlinear, and despite the frequent assumption that accurate brain models must be nonlinear [29], [30], at the macroscale this is not necessarily the case. The recent comparison [27] of a large variety of linear and nonlinear macroscopic models did not find any advantage in the latter. This follows from the linearizing effect of spatial averaging [31], which is reflected in the fact that the nonlinear microscale dynamics converge to linear dynamics at the macroscale, where a significant amount of averaging has occured.

In this work we are interested in discussing computational brain models at the mesoscale, describing the interaction between populations of neurons each having similar function and statistical properties. Two main types of mesoscale models are local field potential models (LFPs) and firing rate models. LFP models are based upon measuring the electric potential in the extracellular space around neuron populations, while firing rate models measure the average firing rate of all the neurons within a population [26]. Both LFPs and firing rate models have been

DYNAMICAL SYSTEMS MODELS IN NEUROSCIENCE

There are two main reasons that a single model is not sufficient for describing the behavior of the brain. The first is size, as the brain is composed of tens of billions of neurons. The second is the complexity of the wide range of behaviors exhibited by the brain. Some involve only a few neurons in a small area, while some involve millions of neurons spread across the brain. As it is infeasible to create an accurate dynamical system model with billions of nodes, it is necessary to use multiple models. These models are generally divided into categories based on the size of their components. Models looking at individual neurons or small groups are "microscale" models, those considering large regions composed of millions of neurons are "macroscale" models, and those in between are referred to as "mesoscale". At each scale there exist a variety of models, which we summarize as follows.

- Microscale models consider the behavior of individual neurons, describing processes such as action potentials. These models are highly nonlinear, and directly consider the currents and voltage differences across membranes. One of the most famous of these models is the Hodgkin-Huxley model [23], originally used to describe the squid giant axon. However, well over a thousand other models exist, and many are collected in the NEURON database [134].
- Macroscale models, designed to model the interactions between large regions in the brain differ significantly from the microscale models. This follows from their definition as the average behavior of large populations, which has been shown to move towards being linear [31]. Commonly used macroscale models include linear models, neural mass models, and recurrent neural networks [27]. A variety of models are also discussed in the review [28].
- Mesoscale models consider populations of neurons that result in networks exceeding microscale models but smaller than the millions of neurons involved in macroscale models. These are generally mean-field models, constructed by averaging the interactions within the population with a single variable. Commonly used models include Local Field Potential models [32], [135] and firing rate models such as sigmoidal [136], [36] or linear-threshold [6], [137] models.

EXAMPLES OF NEURAL ACTIVITIES THROUGH THE LENS OF DYNAMICAL SYSTEMS

In this article we will pay particular attention goal-driven selective attention (GDSA), declarative memory, and epileptic seizure activity.

- GDSA is the process in which the brain actively determines which subset of the currently incoming sensory information is relevant for the current task in order to process it, while simultaneously suppressing irrelevant information. These two components are referred to as *selective recruitment* and *selective inhibition*, respectively. Examples of GDSA include selective vision in busy visual fields, selective listening in a noisy environment, and selective smell. While GDSA has been widely studied in the neuroscience community, see [138], [139], [140], [54], [141], [56], [142], the recent work [6], [7], [85] approaches it from a dynamical systems perspective.
- Epilepsy is a disease of the brain characterized by recurrent seizures. While seizures can take different forms and have varying symptoms, they all include abnormal brain activity, typically either excessive or highly synchronous oscillatory behavior [143]. Seizures have been studied extensively through the dynamical systems perspective with a variety of models [144], [145], [146] and approaches [64], [147], [148], [149], [60], including the linear-threshold model [65], [97]. Dynamical systems approaches to seizures have been effective due to the ability to relate seizures with bifurcations in the network, capturing the sudden switch from healthy to seizure behavior.
- Research of memory models dates back to the late 19th century [150], and are extensive [151], [152], [153] with general divisions between short-term and long-term memory being constant across the literature. By the 1990's, models included further divisions, with working memory being key for short-term memory and long term memory divided into declarative and non-declarative memory [154]. In this paper we consider declarative memory, which is the component of long-term memory that includes the ability to consciously store and retrieve personal information (episodic memory) and general knowledge (semantic memory) [69]. In the 1980's both short and long-term memory models started to be considered using a dynamical systems approach [70], [71], with memories being defined by properties of the dynamics. Since these early studies the modeling of memory has been extensively studied with a systems theory approach [155], [156], [157], [72], [158], motivated by the ability to relate the structure of the network with the observed activity patterns through the models.

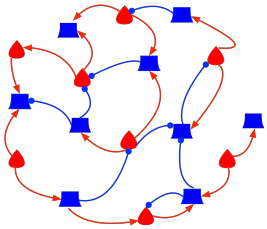

FIGURE 1 Graph-theoretic model of a brain network. Excitatory neurons and connections are shown in red, while inhibitory neurons and populations are shown in blue.

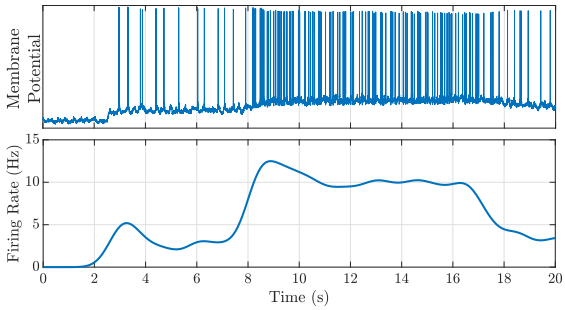

FIGURE 2 An intracellular recording showing a spike train as is used for communication between neurons (top) and the corresponding firing rate (bottom), estimated by binning spikes in 100^{ms} bins and smoothing using a Gaussian window with 500^{ms} standard deviation [6], [132], [133].

used extensively for studying brain function [32], [33], [34] and, in their simplest forms, can be transformed into each other through an affine transformation [35]. In this work, we study firing rate models, in particular the linear-threshold rate model, and its application to multiple brain functions.

In addition to the spatial scale of information in the brain, there exist vast temporal differences between distributed neural processes. Each region/circuit in the brain operates on its own timescale, that might be different to the timescales of other regions and circuits.

As such, when considering a model at any scale of spatial information, it is necessary to encode a timescale into the model dynamics of each region, and examine the impact in the dynamical behavior of their relative differences.

Regardless of the scale of the brain network model, they all have basic graph-theoretic elements in common. A brain network is modeled as a collection of nodes, with nodes representing individual neurons, populations of neurons, or brain regions, depending on the scale of the model. Each of these nodes has its own defining properties (such as consisting of excitatory or inhibitory neurons) and they are connected to form a network structure as shown in Figure 1. Specific model aspects (such as functional forms or parametric constraints) are then defined in accordance with the information scale of the model. Our next section describes the particular assumptions made to describe firing rate models. The reader familiar with these models can safely skip this discussion.

Firing Rate Models

In this section we outline the construction of firing rate models in the brain, as per [26, § 7]. At the level of neurons, brain dynamics consist of a series of spikes, or action potentials, being transmitted between neurons, see Figure 2. The spike train is transmitted from one neuron to another at a *synapse*, and as such the two neurons are referred to as the *pre-synaptic* and *post-synaptic* neurons. The sequence of spikes (both input and output signals) transmitted between neurons is defined by a neural response function, $\rho(t)$, modeled as an impulse train of the form $\rho(t) = \sum_k \delta(t - t_k)$, with δ denoting the Dirac delta function.

In many areas of the brain, the spike trains defined by the neural response function appear to be highly random, and observations have little trial-to-trial reproducibility, which makes accurate spike train models difficult to construct. Replacing the neural response function with the average firing rate provides more trial-to-trial reproducibility (see Figure 2), along with providing some other benefits. First, spiking models can only accurately predict spike trains sequences if all inputs into a neuron are known. Given the complexity of the brain with billions of neurons, knowing this is highly unlikely.

Second, the probability of any two randomly selected neurons being connected is low. Hence, the construction of a network model that has a high degree of connectivity while maintaining this property requires using a large number of nodes. Therefore it is standard practice to instead model a single node in a network model as the average response of a population of neurons. This allows for a less sparse network model. When using spike trains, this practice makes it difficult to describe what the average response of the population is. The use of firing rates instead allows us to specify the average response simply as the average firing rate of the neurons within the population.

We next briefly explain how the firing rate model is constructed. First, we determine how the total synaptic input of a neuron depends on the firing rates of its pre-synaptic afferents. Consider a pair of pre- and post-synaptic neurons, with firing rates given by $x_{\text{pre}}(t)$ and $x_{\text{post}}(t)$. Then, the firing rate of the pre-synaptic neuron generates the synaptic input into the post-synaptic neuron in the form of an electrical current, denoted $I_{\text{post}}(t)$. Assuming the synapse has fast dynamics, $I_{\text{post}}(t)$ is approximately proportional to $x_{\text{pre}}(t)$ with proportionality constant $w_{\text{post,pre}}$, where $w_{\text{post,pre}}$ is known as the synaptic weight. The pre-synaptic neuron is excitatory if $w_{\text{post,pre}} > 0$ and is inhibitory if $w_{\text{post,pre}} < 0$. As such, an excitatory neuron increases the activity of its out-neighbors while an inhibitory neuron decreases it. We note that excitation and inhibition is a property of neurons, rather than synapses, so a neuron either excites or inhibits all of its out-neighbors, but not a combination (this is known as *Dale's law*). The synaptic current of a neuron that receives multiple

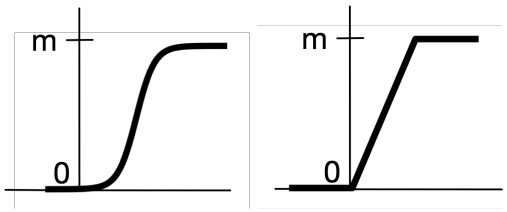

FIGURE 3 The sigmoidal (left) and linear-threshold (right) activation functions are commonly used for defining firing rate models.

synaptic inputs follows a superposition law, with

$$I_{\text{post}}(t) = \sum_j w_{\text{post},j} x_j(t), \tag{1}$$

where the sum is taken over the neurons providing inputs.

Next, we model how the firing rate of the post-synaptic neuron depends on the synaptic input as $x_{\text{post}}(t) = F(I_{\text{post}}(t))$, where $F(\cdot)$ is a nonlinear "activation" function. While a variety of functions can be used for F, the most commonly used are sigmoidal and linear-threshold functions, shown in Figure 3.

Both functions are bounded below, as required for the interpretation that a negative firing rate is physiologically impossible. In addition, they are both bounded above, which is relevant for stabilizing the network against excessively high firing rates. Here, we consider a linear-threshold activation function, giving $x_{\text{post}} = [I_{\text{post}}]_0^m$, with m being the upper bound on the firing rate. The resulting firing rate dynamics from this choice of activation function is

$$\tau \dot{x}_{\text{post}}(t) = -x_{\text{post}} + [I_{\text{post}}(t)]_0^m, \tag{2}$$

where τ is a timescale constant indicating a "lag" between the change in the synaptic input and the change in the firing rate. For simplicity, we assume that $I_{\text{post}}(t)$ is measured in Hz, as such it has a multiplicative constant converting it from the traditional current unit of amperes. In addition, this makes the synaptic weights $w_{\text{post},j}$ dimensionless constants.

While this derivation of a firing rate model as described above uses individual neurons, it is common to replace the individual neurons with populations of neurons with similar activation patterns, resulting in a firing rate model at the mesoscale. In this case, the firing rates x_{pre} and x_{post} represent the average firing rate of the population of neurons. Finally, to move from the dynamics of a single pair of neurons (or populations of neurons) to the dynamics of a brain network, we take the following steps. We consider a network with n nodes and let $\mathbf{x} \in \mathbb{R}^n$ represent the firing rates of the nodes. Then, combining the synaptic weights $w_{i,j}$ into a matrix $\mathbf{W}$ and using (1) and (2), we obtain the network linear-threshold dynamics

$$\tau \dot{\mathbf{x}} = -\mathbf{x} + [\mathbf{W}\mathbf{x} + \mathbf{d}(t)]_{\mathbf{0}}^{\mathbf{m}}. \tag{3}$$

The term $\mathbf{d}(t)$ is added to the synaptic input to model external inputs to the network, such as un-modeled background activity, inputs from other parts of the brain or external sources, or non-zero thresholds. We note that the vector of firing rate upper bounds $\mathbf{m}$ can be modeled as either finite or infinite. While the finite model is biologically sensible, if one assumes that the activity of the network does not approach the typical firing rate threshold, then using an infinite bound (and therefore removing the upper threshold) can be convenient for network analysis.

The linear-threshold model has two significant advantages as a mesoscale model. First, it is weakly nonlinear, which aligns with the gradual linearization of the nonlinear microscale models towards linear macroscale models as averaging is performed over larger populations [31]. Second, the weak nonlinearity in the model, which is piecewise affine, is more analytically tractable than other nonlinear models, such as a sigmoid-based model [36].

Before continuing we note that (3) is not the only form for a firing rate model. Most firing rate models fall into one of the following two forms:

$$\tau \dot{v} = -v + Wf(v) + d(t) \tag{4a}$$

$$\tau \dot{r} = -r + f(Wr + d(t)). \tag{4b}$$

In these equations v and r represent the neural activity, W the synaptic weight matrix, $f(\cdot)$ is a nonlinear, non-negative, input-output function (such as the linear-threshold), and $d(t)$ is any external input. The work [37] shows that these two forms are mathematically equivalent. The requirement that f be non-negative follows from the fact that firing rates are non-negative by definition. If instead f is sign indefinite, the model (4a) can be interpreted as describing membrane potentials [38]. The model (3) that we discuss in this work is of type (4b).

Modeling Different Brain Regions

Since distinct functions involve different areas in the brain, it is important for models to accommodate different structures to describe multiple phenomena and behaviors. A majority of the literature on brain networks studies the cortex and cortical networks [32], [39], [40], [41] due to its role in higher-level processes in the brain, including memory and attention [42]. However, most cortical regions have inputs from subcortical areas, including the thalamus, that play critical roles in the many functions undertaken by the cortex [43], see "The Thalamus - More than a Relay Station" for details.

Given the various functions in which distinct brain regions are involved, homogeneous modeling of all brain regions can be overly simplistic. In order to account for the differences in regional properties, we can impose restrictions at various levels, such as functional forms, hyper-parameters, or parameters, on the sub-models used for different regions. In this work we assume a homogeneous use of the firing rate model with a linear-threshold functional form as derived in (3), and encode regional heterogeneity into the structure of the synaptic weight matrices making up the sub-model corresponding to each region. The following is a description of the constraints we impose on the models of cortical and thalamic regions, respectively.

The cortex is composed of a mix of excitatory and inhibitory neuron populations and, while excitatory neurons significantly outnumber inhibitory neurons, both play important roles in the

THE THALAMUS – MORE THAN A RELAY STATION

The thalamus is a component of many different brain networks and thus plays a role in a large number of functions. Traditionally, the thalamus has been considered primarily as being a sensory relay to the cortex, playing minimal other functional roles [159]. Despite being known since the late 19th century to have additional functions such as a role in memory loss [160], up until recently the majority of the research into thalamic function has studied its function as a sensory relay [43], [161], [162]. This view was gradually changed by several works, including the pioneering work [163], establishing the thalamus as a heterogeneous structure only a small portion of whose nuclei play the role of a sensory relay. Following this work, research has shown that thalamus plays a role in learning and memory [76], attention, impulse control and decision-making [164], [165], motor sequencing [166], and feedforward inhibitory control of cortical regions [164], [167], [47], [168], among others.

Thalamic nuclei can be broadly divided into two categories depending on their role in these applications. Nuclei involved mainly in the role of the thalamus as a sensory relay are known as *first-order* or *specific* and receive their input from other subcortical structures. The thalamic nuclei involved in the variety of other brain functions associated with the thalamus are referred to as *higher-order* or *non-specific* and receive their inputs from varying cortical regions [46]. The higher-order nuclei are then able to directly elicit activity in cortical regions based on the modulation of inputs to the cortex. These divided roles in thalamic function motivate the construction of separate models for explaining their functions in brain networks.

One mechanism for the interaction of thalamus with cortical regions is through feedforward inhibitory control [168], [47], [48]. As such, when studying thalamocortical networks, models need to take into account that many of the net impacts from the thalamus onto cortical regions are inhibitory, while returning connections are both excitatory and inhibitory. In the context of modeling the brain from a control-theoretic perspective, the thalamus provides an exciting avenue of study as an internal controller, modulating and transferring information between cortical regions in parallel to cortico-cortical transmissions.

transmission and processing of information [40]. As such, we allow our firing rate model for cortical regions to be composed of populations of excitatory and inhibitory neurons with arbitrary numbers and connectivity patterns. We only restrict synaptic weight matrices of cortical regions such that outgoing connections from each population are all either excitatory or inhibitory. This is reflected in the matrices such that each column has either nonnegative or nonpositive values [26]. Within the cortex different stimuli are processed in different areas and at different rates. Regions closer to the sensory areas process information faster than those further away, creating distinct temporal hierarchies for stimuli such as visual and auditory [44]. Within the model these hierarchies are reflected by different neurons having different timescales, τ, which combined with the network topology dictate the location of a neuron within the hierarchy.

The *thalamus* connects with cortical regions through a series of parallel pathways, with most thalamic nuclei projecting to a unique cortical population [45]. However, lateral connections within the thalamus (including both excitatory and inhibitory populations, the latter of which lying primarily in the thalamic reticular nucleus) construct the transthalamic pathways between cortical regions that can lie in different places within a hierarchical structure in the cortex [43], [46]. Experimental observations indicate that along these pathways one of the mechanisms through which the thalamus and cortex interact is feedforward inhibition mediated by local interneurons [47], [48], [49].

In particular, these observations show that the cortex receives excitatory thalamic input but is inhibited due to connections between the thalamic input and inhibitory interneurons both for first-order sensory thalamic nuclei [50], [51], [52] and higher-order thalamic nuclei [49].

Given the complexity of thalamic structure, we make the following simplifying assumptions towards its computational modeling. First, we model the thalamus as a single region within the model that can project to any cortical population. With this assumption we are including multiple nuclei within a single region and lateral connections between the thalamic nuclei are included in the internal dynamics. Second, we model the projections (outgoing connections) of the thalamus onto the cortical regions as being strictly inhibitory, mimicking the above-cited experimental observations of feedforward inhibition of the cortex by the thalamus while also simplifying the model. We note that the connections back from the cortical regions to the thalamus are allowed to be both excitatory and inhibitory. Finally, the internal dynamics of the thalamus are restricted only such that each column has a nonpositive or nonnegative sign, similarly to the cortical regions.

Control of Brain Models

Brain models in general, and the simplified and tractable form of firing rate models in particular, are natural pathways to the study of control mechanisms of and for the brain. Akin to engineered systems, the types of control utilized in the brain can be (roughly) separated into feedback and feedforward. Feedback control operates off of circuits where the populations providing the control input are directly stimulated by the populations within the network. In these circuits, the magnitude of the control input is directly dependent on the activity level in the network. On the other hand, feedforward control is not dependent upon current activity levels within the network and is based upon input received from populations of neurons that may be further from the network.

FIGURE 4 Feedback and feedforward mechanisms of control within brain networks. The left panel shows an inhibitory feedback loop, where an excitatory signal (red) from the main neuronal population (grey) stimulates an inhibitory interneuron (blue), which in turn inhibits the main population. The right panel shows the feedforward inhibition mechanism, where an excitatory signal from a separate neuronal population stimulates an inhibitory interneuron as well as the main population. The interneuron then inhibits the main population, typically resulting in its net inhibition.

Feedback control is a mechanism based upon the interaction of two neuronal populations that form a closed loop. While feedback exists across the brain, a large component of feedback control occurs in local feedback loops. In the feedback circuit, the first population stimulates a second "control" population, which in return stimulates the first population in order to control its dynamics. As the "control" neuron population can be either excitatory or inhibitory, both excitatory or inhibitory feedback control exists within the brain. However, despite the existence of more excitatory than inhibitory neurons, the inhibitory neurons frequently exhibit higher firing rates and are able to influence the firing rates of other neuronal populations more than excitatory populations can, see [40]. As such, inhibitory feedback control is more common than excitatory feedback [53]. Figure 4(left) illustrates a standard inhibitory feedback loop.

Feedforward control is more often studied in the context of (potentially unidirectional) non-local connections between neuronal populations. In the case of cortical populations, for instance, they receive afferents from subcortical nuclei (such as the thalamus) as well as cortical populations in distant regions. These long-distance connections may not form clear feedback loops, but instead provide a feedforward control input that can modify the dynamics of the receiving neuronal population. While long-range connections in the brain are almost universally excitatory, they can indeed induce feedforward inhibition by exciting inhibitory "interneurons" (neurons with only local output connections), which in turn inhibit their downstream neuronal population. If this two-hop inhibition is stronger than the direct excitatory afferent received by the downstream population, as is commonly the case, a net feedforward inhibition would occur [53]. Figure 4(right) illustrates the feedforward inhibition mechanism.

ANALYSIS OF INDIVIDUAL BRAIN REGIONS

As outlined in the prior section, at any scale the brain is composed of multiple regions. However, in order to understand the behavior of a model of the overall network, it is beneficial to start by examining the function of the model in individual regions. In this section, we examine the dynamical systems modeling of GDSA, epileptic seizure activity and declarative memory using linear-threshold dynamics (only) of a single region. In the next section, we address more complex scenarios involving networks of networks modeling the interconnection of multiple brain regions. The applications considered here relate to three main properties of the linear-threshold rate dynamics: selective inhibition and recruitment in GDSA relates to stabilizability, epileptic seizure activity relates to bifurcations, and our models of declarative memory are based on multistability of neural dynamics.

We consider a brain region composed of n nodes, with each node representing a population of either excitatory or inhibitory neurons, and governed according to the linear-threshold dynamics in (3). The network structure, shown in Figure 1, is encoded by the synaptic weight matrix $\mathbf{W}$. We begin by formalizing the problem of selective inhibition and recruitment within the framework of linear-threshold firing rate dynamics.

Goal-driven Selective Attention in a Single Brain Region

Selective inhibition and recruitment is the process of identifying task-irrelevant and task-relevant stimuli, and suppressing the task-irrelevant ones while processing the task-relevant ones. Since different stimuli are, to a first approximation, processed by distinct populations of neurons [54], [55], [56], [57] (a fact closely related to the sparseness of the neural code, see [58], [59]), this can be rephrased as inhibiting the populations of neurons associated with the task-irrelevant stimuli and recruiting the populations associated with task-relevant stimuli. As such, for the purpose of considering GDSA from a model-based perspective, we partition both the state variables $\mathbf{x} \in \mathbb{R}^n$ and the synaptic weight matrix $\mathbf{W}$ based upon the task-irrelevant and task-relevant nodes, as follows

$$\mathbf{x}(t) = \begin{bmatrix} \mathbf{x}^0(t) \\ \mathbf{x}^1(t) \end{bmatrix} \qquad \mathbf{W} = \begin{bmatrix} \mathbf{W}^{00} & \mathbf{W}^{01} \\ \mathbf{W}^{10} & \mathbf{W}^{11} \end{bmatrix}. \tag{5}$$

Then, inhibiting the task-irrelevant stimuli corresponds to driving $\mathbf{x}^0$ to $\mathbf{0}$, whereas processing the task-relevant stimuli corresponds to driving $\mathbf{x}^1$ to a desired attractor $\mathbf{x}^1_*$. While the ensuing framework is generalizable to arbitrary attractors, for simplicity of exposition, in our treatment we consider $\mathbf{x}^1_*$ to be a desired equilibrium. Accordingly, we also partition the input $\mathbf{d}(t)$ from (3) as

$$\mathbf{d}(t) = \mathbf{B}\mathbf{u}(t) + \tilde{\mathbf{d}}(t),$$

where

$$\mathbf{B} = \begin{bmatrix} \mathbf{B}^0 \\ \mathbf{0} \end{bmatrix} \qquad \tilde{\mathbf{d}}(t) = \begin{bmatrix} \tilde{\mathbf{d}}^0(t) \\ \tilde{\mathbf{d}}^1(t) \end{bmatrix},$$

resulting in the dynamics

$$\tau \begin{bmatrix} \dot{\mathbf{x}}^0(t) \\ \dot{\mathbf{x}}^1(t) \end{bmatrix} = -\begin{bmatrix} \mathbf{x}^0(t) \\ \mathbf{x}^1(t) \end{bmatrix} + \left[\begin{bmatrix} \mathbf{W}^{00} & \mathbf{W}^{01} \\ \mathbf{W}^{10} & \mathbf{W}^{11} \end{bmatrix} \begin{bmatrix} \mathbf{x}^0(t) \\ \mathbf{x}^1(t) \end{bmatrix} + \begin{bmatrix} \mathbf{B}^0 \\ \mathbf{0} \end{bmatrix} \mathbf{u}(t) + \begin{bmatrix} \tilde{\mathbf{d}}^0(t) \\ \tilde{\mathbf{d}}^1(t) \end{bmatrix} \right]_{\mathbf{0}}^{\mathbf{m}}. \tag{6}$$

This decomposition allows us to separate the inhibition of the task-irrelevant populations from the recruitment of the task-relevant populations. The term $\mathbf{B}^0\mathbf{u}(t)$ allows for the inhibition

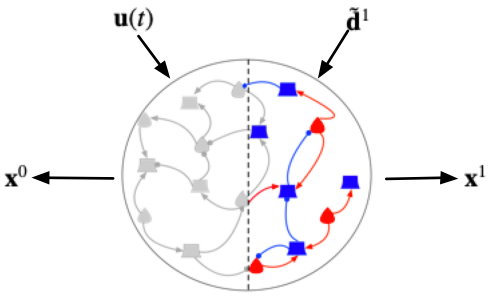

FIGURE 5 Brain region divided into task-irrelevant (grey) and task-relevant (red and blue) neuron populations. The task-irrelevant nodes make up $\mathbf{x}^0$ in the partition of the state, while the task-relevant nodes form $\mathbf{x}^1$. The control input $\mathbf{u}(t)$ is used to selectively inhibit the task-irrelevant populations, while the input $\tilde{\mathbf{d}}^1$ recruits the task-relevant populations to an equilibrium.

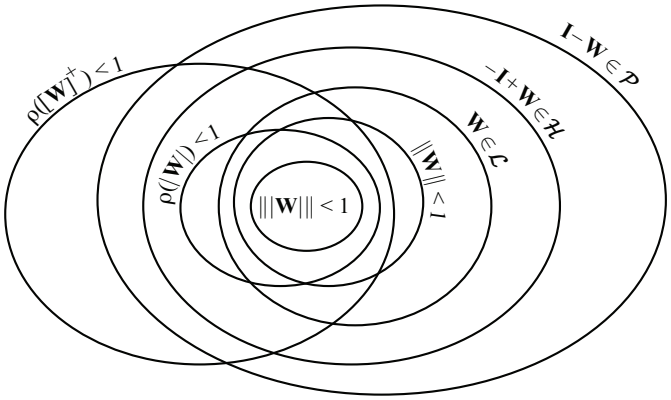

FIGURE 6 Inclusions satisfied by the different matrix classes in Definition 1.

of the task-irrelevant populations through either an external control source or connections with another controlling neuron population. Meanwhile, the term $\tilde{\mathbf{d}}^1(t)$ allows for the recruitment of the task-relevant populations by representing the information pathways between different brain regions along with any additional unmodeled activity impacting the equilibrium to which the task-relevant components are recruited. Figure 5 illustrates the discussion above.

With these decompositions in place, the problem of selective inhibition and recruitment of the network can now be formulated mathematically as follows: under what conditions on the network structure can we find control $\mathbf{u}(t)$ such that the network dynamics are stabilizable to $(\mathbf{0}, \mathbf{x}_1^*)$?

Stability of Linear-Threshold Networks as a Function of Interconnection Structure

The ability to achieve selective inhibition and recruitment depends on the stabilizability of the network through feedforward and feedback control mechanisms. Understanding stabilizability, in turn, requires understanding the stability properties of the dynamics, and how the interconnection structure of the network affects it. Our ensuing discussion tackles this point.

For simplicity, we assume that the input term is constant, $\mathbf{d}(t) = \mathbf{d}$, before generalizing the discussion to time-varying $\mathbf{d}(t)$ subsequently. The stability properties of the dynamics are closely related to its network structure, which in the linear-threshold brain model is encoded into the synaptic connectivity matrix $\mathbf{W}$. As such, we introduce the following notions of matrix classes.

Definition 1

A matrix $\mathbf{W} \in \mathbb{R}^{n\times n}$ is

- » *absolutely Schur stable* if $\rho(|\mathbf{W}|) < 1$ where $\rho(\cdot)$ is the spectral radius;
- » *totally $\mathcal{L}$-stable* ($\mathbf{W} \in \mathcal{L}$) if there exists $\mathbf{P} = \mathbf{P}^\top > \mathbf{0}$ such that for all $\sigma \in \{0,1\}^n$

$$(-\mathbf{I} + \mathbf{W}^\top\Sigma)\mathbf{P} + \mathbf{P}(-\mathbf{I} + \Sigma\mathbf{W}) < \mathbf{0},$$

where $\Sigma = \mathrm{diag}(\sigma)$;

- » *totally Hurwitz* ($\mathbf{W} \in \mathcal{H}$) if all its principal submatrices are Hurwitz;
- » a *P-matrix* ($\mathbf{W} \in \mathcal{P}$) if all its principal minors are positive.

We note that these matrix classes are related to each other through a variety of inclusions, as shown in Figure 6.

Using these matrix classes, we can provide conditions for both the existence and uniqueness of equilibria (EUE) and global exponential stability (GES) of the dynamics

$$\tau\dot{\mathbf{x}} = -\mathbf{x} + [\mathbf{W}\mathbf{x} + \mathbf{d}]_{\mathbf{0}}^{\mathbf{m}}.$$

In particular, following [6], the dynamics have a unique equilibrium point if and only if $\mathbf{I} - \mathbf{W} \in \mathcal{P}$, are locally asymptotically stable only if $-\mathbf{I} + \mathbf{W} \in \mathcal{H}$, and are GES if $\mathbf{W} \in \mathcal{L}$. Further, based on extensive simulations, [6] conjectures that $-\mathbf{I} + \mathbf{W} \in \mathcal{H}$ is necessary and sufficient for GES. One challenge with using these results, however, is that determining that matrices are P-matrices or totally Hurwitz is computationally challenging, especially as the scale of the network increases. As such, the inclusions in the matrix classes from Figure 6 take on importance as they can be used to construct more conservative conditions (such as the conditions based on the spectral radius and norm of $\mathbf{W}$) for EUE and GES that are computationally tractable.

Achieving Selective Inhibition and Recruitment through Feedforward and Feedback

Given the importance of feedforward and feedback control for the brain we consider achieving selective inhibition and recruitment using both mechanisms. Here, we characterize first each mechanism separately and later discuss the advantages of the combinations thereof.

We begin by considering feedforward inhibition. In this case, the brain region under consideration is being inhibited by a separate (not explicitly modeled here) brain region to an activity/inactivity pattern of its choice through the control input $\mathbf{u}(t)$. Since the linear-threshold activation function is unaffected by excessive inhibition due to its thresholding at zero,

selective inhibition through feedforward inhibition is possible by using a sufficiently strong inhibitory input. Utilizing this we can formalize the following conditions for selective inhibition and recruitment.

Theorem 1

(Selective Inhibition and Recruitment through Feedforward Inhibition [6, Theorem V.2]): Consider a brain region modeled with the linear-threshold dynamics in (6). Suppose that $\dim(\mathbf{u}(t)) \geq \dim(\mathbf{x}^0)$ and that $\text{range}([\mathbf{W}^{00} \;\; \mathbf{W}^{01}]) \subseteq \text{range}(\mathbf{B}^0)$. Then, for any constant $\tilde{\mathbf{d}}^1$, there exists a constant feedforward control input $\mathbf{u}(t) = \bar{\mathbf{u}}$ that stabilizes the dynamics to the unique equilibrium of the form $(\mathbf{0}, \mathbf{x}^*)$ if and only if $\mathbf{W}^{11}$ is such that the internal dynamics

$$\tau \dot{\mathbf{x}}^1 = -\mathbf{x}^1 + [\mathbf{W}^{11}\mathbf{x}^1 + \tilde{\mathbf{d}}^1]_{\mathbf{0}}^{\mathbf{m}^1}$$

is GES to a unique equilibrium.

We discuss the interpretation of the conditions of this result at the end of the section, in parallel with the feedback inhibition case. We note that in Theorem 1 the potential for selective inhibition and recruitment is predicated on the stability of the uncontrolled portion of the dynamics. This illustrates that the properties required for selective inhibition and selective recruitment can be fully separated. The ability for selective inhibition is based upon the dynamics for the task-irrelevant nodes, while selective recruitment is based upon only the dynamics of the task-relevant nodes, with no intersection. In a similar fashion, for selective inhibition and recruitment using feedback inhibition, the conditions are dependent only upon the structure of the task-relevant component of the synaptic weight matrix, and are given as follows.

Theorem 2

(Selective Inhibition and Recruitment through Feedback Inhibition [6, Theorem V.3]): Consider a brain region modeled with linear-threshold dynamics in (6) and suppose that $\tilde{\mathbf{d}}^0(t) = \mathbf{0}$. Let the input $\mathbf{u}(t)$ be given by the linear feedback $\mathbf{u}(t) = \mathbf{K}\mathbf{x}(t)$, where $\mathbf{K}$ is a constant control gain and suppose $\dim(\mathbf{u}(t)) \geq \dim(\mathbf{x}^0)$. Further, assume that $\text{range}([\mathbf{W}^{00} \;\; \mathbf{W}^{01}]) \subseteq \text{range}(\mathbf{B}^0)$. Then, there almost always exists a $\mathbf{K}$ such that i)

1) $\mathbf{I} - (\mathbf{W} + \mathbf{B}\mathbf{K}) \in \mathcal{P}$ if and only if $\mathbf{I} - \mathbf{W}^{11} \in \mathcal{P}$;
2) $-\mathbf{I} + (\mathbf{W} + \mathbf{B}\mathbf{K}) \in \mathcal{H}$ if and only if $-\mathbf{I} + \mathbf{W}^{11} \in \mathcal{H}$;
3) $\mathbf{W} + \mathbf{B}\mathbf{K} \in \mathcal{L}$ if and only if $\mathbf{W}^{11} \in \mathcal{L}$;
4) $\rho(|\mathbf{W} + \mathbf{B}\mathbf{K}|) < 1$ if and only if $\rho(|\mathbf{W}^{11}|) < 1$;
5) $\|\mathbf{W} + \mathbf{B}\mathbf{K}\| < 1$ if and only if $\|[\mathbf{W}^{10} \;\; \mathbf{W}^{11}]\| < 1$.

The interpretation of each of the results in Theorem 2 is as follows. First, recalling that selective inhibition and recruitment occurs when the system is stabilizable to a unique equilibrium $(\mathbf{0}, \mathbf{x}^*)$, Theorem 2*i*) guarantees the existence and uniqueness of the equilibrium $\mathbf{x}^*$ for the task-relevant components. However, this condition does not guarantee the equilibrium is stable, so it is not sufficient for selective inhibition and recruitment. Theorem 2*ii*) then guarantees local asymptotic stability (and potentially GES) of the equilibrium point $\mathbf{x}^*$. The remaining conditions utilize the matrix inclusions given in Figure 6 to provide sufficient conditions for stabilizability of the task-relevant conditions to the equilibrium $\mathbf{x}^*$. Theorem 1*iii*) guarantees GES of the task-relevant components of the dynamics to $\mathbf{x}^*$, thus providing a sufficient condition, when combined with the assumptions of the result, that selective inhibition and recruitment is achievable through stabilization to $(\mathbf{0}, \mathbf{x}^*)$. Condition *iv*) does not guarantee GES, as the matrix class $\rho(|\cdot|) < 1$ is not a subset of the class of $\mathcal{L}$-stable matrices, but it is more computationally tractable and does guarantee local asymptotic stability. Finally, Theorem 2*v*) is computationally tractable, and is sufficient for guaranteeing GES of the equilibrium $\mathbf{x}^*$, allowing for stabilizability to $(\mathbf{0}, \mathbf{x}^*)$.

To conclude this section, we discuss the assumptions in Theorems 1 and 2. Both the feedforward and feedback case require an assumption on the relationship between the range of the task-irrelevant component of the synaptic weight matrix and the task-irrelevant component of the inhibitory control matrix $\mathbf{B}^0$. In both results, the purpose of this condition is to guarantee the existence of a control allowing the result to hold. In the feedforward inhibition result, it guarantees the existence of the constant control $\mathbf{u}$ used to achieve inhibition, while in the feedback inhibition result, it guarantees the existence of the matrix $\mathbf{K}$. The second assumption is that the dimension of the control is at least as large as the number of task-irrelevant nodes in the system. Intuitively, this result guarantees that the control can inhibit every task-irrelevant node in the system (it would not be possible to achieve this if the dimension was smaller).

Epileptic Seizures through Bifurcations in a Single Brain Region

Epilepsy is a neurological disease characterized by chronic unprovoked seizures. While epilepsy can be caused by many different factors and there are multiple types of seizures, seizures typically correspond to a sudden change from healthy to unhealthy activity. As such, when studying epilepsy from a dynamical systems perspective, the emergence of seizures can be modeled through bifurcations in the model [60], [61]. In this section, we look at phrasing epileptic events using bifurcations in the model of a single brain region. In particular, using linear-threshold dynamics (3), consider an excitatory-inhibitory pair (here $n = 2$)

$$\tau \dot{\mathbf{x}} = -\mathbf{x} + [\mathbf{W}\mathbf{x} + \mathbf{u}]_{\mathbf{0}}^{\mathbf{m}}, \tag{7}$$

where the synaptic weight matrix $\mathbf{W}$ and input $\mathbf{u}$ are

$$\mathbf{W} = \begin{bmatrix} a & -b \\ c & -d \end{bmatrix} \qquad \mathbf{u} = \begin{bmatrix} u_1 \\ u_2 \end{bmatrix}, \tag{8}$$

with $a, b, c, d \in \mathbb{R}_{>0}$ and $u_1, u_2 \in \mathbb{R}$. Since we are studying a single region, we are considering focal seizures, but in the following we will consider the idea of generalized seizures through the spread of epileptic behavior across networks.

Electroencephalography (EEG) is one of the most commonly used tools for measuring and viewing brain activity, particularly for the diagnosis and study of epilepsy. As such, when taking a dynamical systems approach to studying epilepsy, it is common to assume that the activity (output) of the dynamical system represents (abstracted and simplified) EEG signals [62]. During both healthy and unhealthy activity a variety of behaviors appear in the EEG measurements. However, a number of types of waveforms have been commonly observed during epileptic seizures [63]. These waveforms can then be used as a basis to approximate an EEG response. One can then relate each of these waveform types to specific properties of a dynamical system being used to model EEG signals [64]. The types of waveforms and the dynamical system properties we use to model them are summarized as follows.

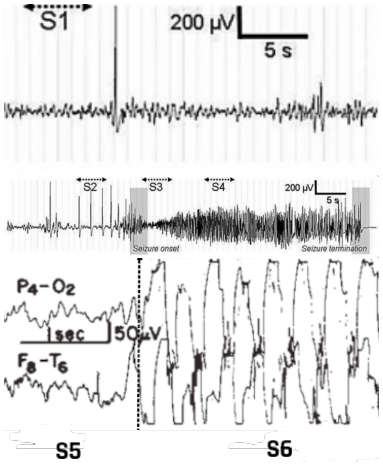

FIGURE 7 EEG recording of an epileptic waveform [93]. Sections of the waveforms are labeled according to the activity types described in Remark 1. S1 corresponds to healthy background activity, S2 to low frequency spikes, S3 to irregular high frequency oscillations and S4 to quasi-sinusoidal low-frequency oscillations. S5 and S6 correspond to high frequency oscillations and slow waves, respectively [63].

Remark 1

(Waveforms Observed in EEG Recordings): The following waveform types are commonly observed in EEG signals, and we discuss them based on the seizure shown in Figure 7, with regions divided based on the qualitative changes in behavior.

1) Background activity (S1 in Figure 7): This is characterized by low-amplitude fluctuations or oscillations around a mean-centered steady state value. This activity generally lies in the theta band ($4-7$ Hz) [64]. In terms of a dynamical systems representation we model the background activity as the network having a equilibrium. In this case the model behavior will stay in the area of the equilibrium, fluctuating based upon noise in the system [64].
2) Epileptic Spiking (S2): These are isolated non-rhythmic spikes and are commonly observed sporadically prior to seizures during otherwise healthy background activity [64]. In modeling these from a dynamical systems perspective, they appear when the system is multistable, with one of the equilibria being the origin. The spikes then appear when the system activity moves into the orbit of the non-zero equilibrium [65].
3) Irregular low amplitude oscillations (S3): These significantly higher frequency oscillations than those seen in background activity, with a dominant frequency in the range of $20-40$ Hz [64]. In the seizure shown in Figure 7 these appear at the onset of the seizure, with the brain activity suddenly and significantly increasing in frequency from the background activity and spikes seen in S1 and S2. We have two approaches to modeling this with a dynamical system. First, as oscillations they can be modeled as limit cycles in the dynamics [64]. The other option, due to the irregularity in the oscillations, is to model them as the dynamics being multistable, with the irregular oscillations appearing as the movement of the system between the orbits [65].
4) Quasi-sinusoidal oscillations and rhythmic spiking (S4): These are higher amplitude oscillations that begin at a high frequency but slow down into a rhythmic spiking pattern. The rhythmic spiking typically lies in the alpha band, with a dominant frequency near 10 Hz [64]. In Figure 7 these appear as the seizure develops, with the activity slowing down from the the oscillations seen in S3. These are modeled using stable limit cycles in the dynamics [64].
5) Slow waves (S6): These are very low-frequency ($1-2.5$ Hz [63]) high amplitude waves with intermittent spikes that typically only appear during sleep, but are also observed in epileptic patients both preceding and following seizures [21]. We choose to model these using a combination of an unstable equilibrium and a limit cycle, with the spikes appearing as the system moves between these states [65].

With this relation between EEG waveforms and dynamical systems properties we can now frame the problem of discussing seizures using bifurcations and linear-threshold dynamics. First, what type of bifurcations can occur in the model (7) and what components of a seizure do they correspond with? Second, under what structural conditions on $\mathbf{W}$ and input conditions on $\mathbf{u}$ can EEG waveforms be achieved that qualitatively resemble what is observed during epileptic seizures?

Bifurcations in Linear-Threshold Rate Dynamics

In order to relate bifurcations in the LTR model of a brain network to the EEG activity preceding, during, and following epileptic seizures, we first need to understand how and when bifurcations occur in the dynamics. In this section we will explain both the types of bifurcations that occur in LTR dynamics and structural conditions under which they occur. We begin with a closer look at the structure of the LTR dynamics.

One of the benefits of the linear-threshold network model

is that the nonlinearities in the model are switched-linear. In particular, the dynamics form a piecewise-affine state-dependent switched system, which allows for applying linear analysis within each switching region. Further, this form allows for an elegant characterization of bifurcations occurring in the network, as the qualitative changes in behavior occur as network equilibria move across switching boundaries.

At each point in time, each node in the network can be in one of three states: inactive ($(\mathbf{W}\mathbf{x}+\mathbf{u})_i \leq 0$), linearly active ($(\mathbf{W}\mathbf{x}+\mathbf{u})_i \in (0,\mathbf{m}_i)$), or saturated ($(\mathbf{W}\mathbf{x}+\mathbf{u})_i \geq \mathbf{m}_i$). Therefore at any point in time the network state can be associated with a switching index $\sigma = \sigma(\mathbf{x}) \in \{0,\ell,s\}^n$, where $0,\ell,s$ correspond to a node being inactive, linearly active and saturated, respectively. The indices then define the switching regions for the linear-threshold dynamics as follows

$$\Omega_\sigma = \left\{ \mathbf{x} \in [\mathbf{0},\mathbf{m}] \;\middle|\; \begin{cases} (\mathbf{W}\mathbf{x}+\mathbf{u})_i \leq 0 & \text{if } \sigma_i = 0, \\ 0 \leq (\mathbf{W}\mathbf{x}+\mathbf{u}) \leq \mathbf{m}_i & \text{if } \sigma_i = \ell, \\ (\mathbf{W}\mathbf{x}+\mathbf{u})_i \geq \mathbf{m}_i & \text{if } \sigma_i = s \end{cases} \right\}.$$

Within each switching region Ω_σ, we have that $[\mathbf{W}\mathbf{x}+\mathbf{u}]_{\mathbf{0}}^{\mathbf{m}} = \Sigma^\ell(\mathbf{W}\mathbf{x}+\mathbf{u}) + \Sigma^s\mathbf{m}$, in which Σ^ℓ and Σ^s are diagonal matrices with $\Sigma^\ell_{ii} = 1$ if $\sigma_i = \ell$ and $\Sigma^s_{ii} = 1$ if $\sigma_i = s$. Applying this to the dynamics (7), we get the piecewise-affine form take the form

$$\tau\dot{\mathbf{x}} = (-\mathbf{I} + \Sigma^\ell\mathbf{W})\mathbf{x} + \Sigma^\ell\mathbf{u} + \Sigma^s\mathbf{m}. \tag{9}$$

With the piecewise-affine dynamics, each input $\mathbf{d}$ and switching region σ corresponds with a unique equilibrium candidate $\mathbf{x}^*_\sigma(\mathbf{d})$ given by

$$\mathbf{x}^*_\sigma = (\mathbf{I} - \Sigma^\ell\mathbf{W})^{-1}(\Sigma^\ell\mathbf{u} + \Sigma^s\mathbf{m}). \tag{10}$$

In order to guarantee the equilibrium candidates are well-defined we require the assumption that $\det(\mathbf{W}) \neq 0$ and $\det(-\mathbf{I} + \Sigma^\ell\mathbf{W}) \neq 0$ for all $\sigma \in \{0,\ell,s\}^2$. However, this assumption is not a restriction as the set of matrices not satisfying the assumption has measure zero [6]. Each equilibrium candidate is then an equilibrium of the system if $\mathbf{x}^*_\sigma$ actually belongs to Ω_σ. It is of interest to note that the switching regions Ω_σ are dependent on both the system structure and input. As such, as the input to the system varies the switching regions themselves are changing, which differs from standard state-dependent switched systems. These changing regions result in the dynamics exhibiting richer behavior but correspondingly complicates the analysis. With this form of the dynamics in hand we are ready to discuss bifurcations in the linear-threshold dynamics for the purpose of modeling seizures.

In the excitatory-inhibitory linear-threshold network (7), bifurcations arise due to the piecewise-affine form of the network and are characterized as a function of the network input, $\mathbf{u}$ [65], which is referred to as the bifurcation parameter. Bifurcations then have the opportunity to occur when equilibrium candidates from multiple switching regions coincide for a given value of the bifurcation parameter. Such bifurcations are formalized as follows.

Definition 2

(Bifurcations in Linear-Threshold Networks [65]): A bifurcation parameter $\mathbf{u}$ is called a *bifurcation candidate* for the linear-threshold dynamics (7) if $\mathbf{x}^*_{\sigma_1}(\mathbf{u}) = \mathbf{x}^*_{\sigma_2}(\mathbf{u})$ for $\sigma_1 \neq \sigma_2$. A *boundary equilibrium bifurcation (BEB)* occurs at a bifurcation candidate $\mathbf{u}$ if $\mathbf{x}^*_{\sigma_1}(\mathbf{u}) \in \Omega_{\sigma_1}$ and $\mathbf{x}^*_{\sigma_2}(\mathbf{u}) \in \Omega_{\sigma_2}$.

Now, while we have determined when a bifurcation exists and occurs within the linear-threshold network, there are multiple types of bifurcations. These correspond with different changes in dynamical behavior of the network, and as such can be related to transitions between different waveform types in the EEG. The types of BEBs are defined as follows.

Definition 3

(Types of Boundary Equilibrium Bifurcations [65]): If a boundary equilibrium bifurcation occurs at input $\mathbf{u}$ it is called a

1) a persistent BEB (P-BEB) if the number of equilibria is constant in a neighborhood of $\mathbf{u}$;
2) a non-smooth fold BEB (NSF-BEB) if the number of equilibria is not constant in a neighborhood of $\mathbf{u}$;
3) a Hopf bifurcation if it is locally a NSF-BEB such that a limit cycle emerges globally.

With these types of bifurcations in hand, we are now able to classify qualitative changes in the behavior of the linear-threshold dynamics. However, to understand the dynamics, and to be able to use it to model seizure behavior, it is desirable to have conditions such that each type of bifurcations occur.

We will operate with only a single bifurcation parameter, rather than the two inputs that are part of the model. That is, we will vary the parameter u_1 to achieve bifurcations while maintaining u_2 to be a constant. This is called a codimension 1 bifurcation, and occur more frequently in biological systems than higher-order bifurcations [66]. The following set of inequalities provide conditions for the types of bifurcations in Definition 3 to occur.

Theorem 3

(Conditions for Boundary Equilibrium Bifurcations [65]): Consider an excitatory-inhibitory pair governed by the linear-threshold dynamics (7) with synaptic weight matrix (8). Let $\mathbf{u}$ be the input and assume that u_2 is constant, while u_1 is the bifurcation parameter. Suppose that

$$-\mathbf{m}_1 c < u_2 < (1+d)\mathbf{m}_2.$$

The following inequalities result in four different bifurcation behaviors in the system:

$$a < 1, \tag{11a}$$

$$(a-1)(d+1) < bc, \tag{11b}$$

$$a < d+2. \tag{11c}$$

The bifurcation possibilities are as follows:

(A) if (11a) is satisfied, there exists a unique equilibrium for every input $\mathbf{u}$ and all bifurcations are P-BEB;
(B) if (11a) and (11b) are not satisfied, then the system has either one or three equilibria. Any bifurcations involving the $\Omega_{\ell\ell}$ region and one other region are P-BEB. Any other bifurcations are NSF-BEB;
(C) if (11a) is not satisfied while (11b) and (11c) are, then bifurcation candidates involving Ω_{00} or Ω_{ss} and one other region are P-BEB. Any other bifurcations are NSF-BEB;
(D) if (11b) is satisfied while (11a) and (11c) are not, then the bifurcations are the same as in case (C) except a Hopf bifurcation occurs at $\mathbf{u}_{00}^{\ell 0}$ and at $\mathbf{u}_{ss}^{\ell s}$.

From Definition 3, we see that the properties of bifurcations depend on the number of equilibria and their stability properties. As such, Theorem 3 leverages this observation by determining conditions for the equilibrium candidates, defined by (10), to be actual equilibria, along with their stability properties, resulting in the characterization for the appearance of the different types of bifurcations.

Theorem 3 shows that bifurcation behavior in linear-threshold networks is highly dependent on the structure of the network in addition to the actual bifurcation parameter. As such, when considering how to represent seizure behavior using the linear-threshold model it is important to ensure that the specific network considered has a structure that permits the wide variety of behavior observed in the EEG of epileptic patients.

Constructing Seizure Behavior with Linear-Threshold Bifurcations

In order to use bifurcations in the network to represent seizure behavior, we need to relate the types of bifurcations given in Definition 3 with the EEG waveforms from Remark 1. This is done by matching the dynamical systems properties of the EEG waveform types from [64] with the properties of each bifurcation types. Table 1 proposes a relationship between the types of bifurcations in the network and the types of waveforms that make up both healthy and epileptic EEG behavior.

From Table 1, we can see that bifurcations in the excitatory-inhibitory network governed by linear-threshold dynamics can result in all of the waveform types that appear in the EEG from Remark 1. Note, however, that due to the structural constraints on bifurcation types provided in Theorem 3, not all excitatory-inhibitory pairs exhibit the range of EEG behaviors discussed in Remark 1, and as such are not useful for exhibiting epileptic behavior. This allows, in at least two ways, a realistic representation of modeling epileptic dynamics using LTR models. First, it does not make sense for any arbitrarily constructed network to be a reasonable model for the brain. As such the existence of structural requirements for a network to be able to exhibit specific behavior is expected. Second, seizures generally begin in specific areas of the brain and then either remain there (focal seizures) or spread throughout the brain (generalized seizures) [67]. This, together with the fact that not all people exhibit epileptic symptoms further explains the existence of specific structural conditions for the emergence of epileptic dynamics in the model.

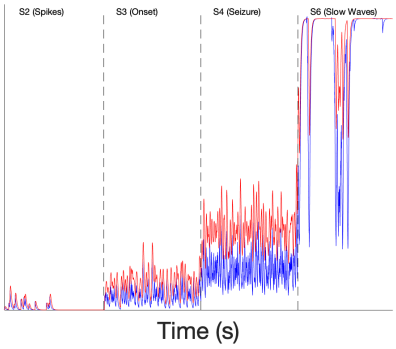

FIGURE 8 Basic epileptic waveforms (as in Figure 7) replicated from an excitatory-inhibitory pair with LTR dynamics, as shown in (12).

We next give an example of using an excitatory-inhibitory pair governed by the linear-threshold dynamics to replicate the seizure behavior seen in Figure 7 through bifurcations. We will use the relations between bifurcation and waveform types from Table 1 to construct the desired waveforms. We further extend the deterministic linear-threshold dynamics in (7) as follows

$$\tau\dot{\mathbf{x}} = -\mathbf{x} + [\mathbf{W}\mathbf{x} + \mathbf{v} + \mathbf{w}]_{\mathbf{0}}^{\mathbf{m}}. \tag{12}$$

Here the input $\mathbf{u}$ is divided into components $\mathbf{v}$ and $\mathbf{w}$, where $\mathbf{w}$ is a white noise input used to simulate the noise content of EEG signals [68]. We construct the synaptic weight matrix $\mathbf{W}$ such that the structural conditions of part (D) in Theorem 3 are satisfied. In Figure 8 we show how the network exhibits each of the waveform types by moving through bifurcations by changing the bifurcation parameter $v_1 + w_1$ while the input $v_2 + w_2$ is fixed at 0. Four main behaviors appear in the network, corresponding with the regions seen in Figure 7.

If the input to the network satisfies $v_1 + w_1 < 0$, the network has a stable equilibrium point at zero which is corresponding to healthy background activity and is not shown in the plot. Approaching $v_1 + w_1 > 0$ is the first bifurcation as when $v_1 + w_1 > 0$ the system has a unique limit cycle. This is a NSF-BEB bifurcation and results in the spikes shown in section S2 of the graph. Further increasing the bifurcation parameter reaches a Hopf bifurcation and gives the small oscillations in S3, and further increasing of the input results in the higher magnitude oscillations of S4 and S5. At the boundary of S5 and S6 we reach a second Hopf bifurcation to move from high amplitude oscillations to the slow waves seen in S6. Further increasing of the bifurcation parameter would result in a NSF-BEB bifurcation that would result in a stable equilibrium point at the upper threshold of the network and correspond to healthy activity.

We end this section by noting that the bifurcation results presented here could be used to inform clinical applications.

TABLE 1 Relation between the type of bifurcation and the change in EEG waveform behavior for networks satisfying the structural conditions in Theorem 3 as defined by Remark 1 [65].

Network Structure	Initial Behavior	Bifurcation	Resulting Behavior
(A)	Healthy background	P-BEB	Healthy background
(B)	Healthy background	P-BEB	Healthy background
(C)	Healthy background	NSF	Spikes
	Spikes	NSF	Healthy background
(D)	Healthy background	NSF	Spikes
	Spikes	Hopf	Oscillations
	Oscillations	Hopf	Slow waves
	Slow waves	NSF	Healthy background

Based on Table 1, P-BEB bifurcations only appear in healthy behavior. Instead, NSF bifurcations are associated with transitions between healthy behavior and epileptic spikes. There are two ways in which the conditions for NSF bifurcations given in Theorem 3 could be useful, depending on whether the therapeutical actuation affects the inputs to the network or the network parameters. In the first case, if epileptic spikes are observed to be appearing in the brain, the appropriate bifurcation parameter could be modified (increased or decreased, depending on specific conditions as determined by the result) in order to result in the NSF bifurcation causing a shift from spikes to healthy behavior. In the second case, if the current input (bifurcation parameter) has resulted in a NSF bifurcation from healthy behavior to spikes, an intervention could seek to temporarily alter the network weights in order to move the network back into healthy behavior until the input changes.

Declarative Memory in Single Region Linear-Threshold Rate Models

Declarative memory is the process of encoding and storing data in the brain, while allowing for the conscious retrieval of that data [69]. In early dynamical system representations of memory, such as [70], [71], memories are encoded and saved as attractive equilibrium points. The retrieval of a memory by the model is represented by the system state reaching a particular equilibrium based on the presentation of specific inputs. In constructing dynamical system models for memory, we look for them to have some specific properties. These include the ability to encode multiple memories and the ability to retrieve specific memories from a partial or corrupted input. Encoding multiple memories (or the capacity of the model) corresponds to having multiple attractive equilibrium points, which can be either forced or unforced, depending on the model. Retrieval from partial inputs is important as it corresponds with a degree of robustness in recovering memories.

In this section, we model memory with a threshold-linear dynamical system, that is, the linear-threshold model without an upper saturation bound, and focus on the ability to encode multiple memories. While the saturating linear-threshold model (3) is a more accurate representation, the upcoming results are not readily generalizable to the saturating model. For modeling memory, we utilize the idea of the support for defining memories. For a state variable $\mathbf{x} \in \mathbb{R}^n$, let the support of the vector be the subset of nodes with non-zero activity, that is

$$\text{supp}(\mathbf{x}) = \{i \in \{1, \dots, n\} \mid \mathbf{x}_i \neq 0\}.$$

We now provide a definition of a memory in this model.

Definition 4

(Memory): Consider a brain network composed of n nodes with synaptic weight matrix $\mathbf{W}$ governed by the threshold-linear dynamics as follows

$$\tau \dot{\mathbf{x}} = -\mathbf{x} + [\mathbf{W}\mathbf{x} + \mathbf{d}]_{\mathbf{0}}^{\infty}. \tag{13}$$

A set $\sigma \subseteq \{1, \dots, n\}$ is a memory in the network if there exists an input $\mathbf{d}$ such that there is a stable equilibrium point $\mathbf{x}^*$ with $\text{supp}(\mathbf{x}^*) = \sigma$.

The reason for using a memory as a set rather than as a single equilibrium point as in [70] is input independence. Unlike the earlier models where equilibrium points remained the same for small changes in the input, the equilibrium points of the threshold-linear model often change with any change in the input. This is undesirable, as inputs are supposed to provide cues for what memory should be invoked, rather than changing the memory itself. Using the support of the vector instead of the equilibrium point provide the desired invariance under similar inputs, as there is always a small enough change in the input such that the support remains the same for the resulting equilibrium point(s).

As retrieval of a memory corresponds with the network reaching the equilibrium point associated with that memory, we note that for this model to "hold" a memory, the input must remain present, which differs from other memory models such as Hopfield [70]. While this may initially seem like a disadvantage, in the context of declarative memory there is no issue. Since declarative memory is a conscious process, while a memory is being accessed, the input cue will be present. Maintaining the memory without an input would instead correspond with an unconscious process.

In what follows, we address two problems related to memory in this model. First, under what conditions on the network structure $\mathbf{W}$ does the network admit the ability to encode multiple memories? Second, for a given set $\sigma \subseteq \{1, \dots, n\}$ and network structure $\mathbf{W}$, does there exist an input $\mathbf{d}$ such that σ

represents a memory that can be encoded and retrieved by the network?

Multiple Memories in Symmetric Threshold-Linear Networks

The ability of a network to encode multiple memories is directly related to the ability of the network to admit multiple stable equilibria. In particular, a network must admit stable equilibrium points with different supports in order to encode multiple memories. As such, we introduce the following notion of permitted and forbidden sets to distinguish whether or not a memory can be encoded on a given set.

Definition 5

(Permitted and Forbidden Sets [72]): Consider a brain network composed of n nodes with synaptic weight matrix $\mathbf{W}$ governed by the threshold-linear dynamics (13). A set of neurons $\sigma \subseteq \{1, \ldots, n\}$ is called *permitted* if for some input $\mathbf{d}$ there exists a stable equilibrium point $\mathbf{x}^*$ with $\text{supp}(\mathbf{x}^*) = \sigma$. A set of neurons is called *forbidden* if it is not permitted.

From this, we have that a memory can only be encoded on a permitted set, and with memories defined by Definition 4, it requires multiple distinct permitted sets to encode multiple memories. Due to this requirement, the existence of multiple stable equilibria is not sufficient for the encoding of multiple memories. This is since the equilibria could form a continuum lying only on a line or surface, which have the same support, and as such are part of the same permitted set. In this case, we can have a network with only one permitted set, and as such only one possible memory. In order to have multiple permitted sets, and as such, memories, we introduce the property of conditional multiattractiveness.

Definition 6

(Conditionally Multiattractive [72]): A network governed by the threshold-linear dynamics (13) is *conditionally multiattractive* if there exists an input $\mathbf{d}$ such that the set of stable equilibrium points is disconnected.

If a network is conditionally multiattractive, then we can guarantee the ability to encode multiple memories, as the disconnected stable equilibrium points will lie in distinct permitted sets. As noted above, a network being multiattractive differs slightly from being multistable. In particular, all multiattractive networks are multistable, but not all multistable networks are multiattractive, by virtue of excluding line and surface attractors.

Before addressing conditions for multiattractiveness in threshold-linear dynamics we return to addressing convergence to an equilibrium through network interconnection structure. We recall that there exists a unique equilibrium point for each input if and only if $\mathbf{I} - \mathbf{W} \in \mathcal{P}$ [6]. However, due to the desire for multiple in this section we desire a slightly more general condition. For this we introduce the notion of copositivity.

Definition 7

(Copositive [72]): A symmetric matrix $\mathbf{W} \in \mathbb{R}^{n \times n}$ is called copositive if $\mathbf{x}^\top \mathbf{W} \mathbf{x} > 0$ for all $\mathbf{x} \in \mathbb{R}^n_{\geq 0} \backslash \{\mathbf{0}\}$. An equivalent condition is that all positive eigenvectors of all submatrices of $\mathbf{W}$ have positive eigenvalues.

With the definition of copositivity in hand, we are able to provide a condition guaranteeing convergence to an equilibrium for threshold-linear networks with symmetric synaptic weight matrices $\mathbf{W}$. In particular, the symmetric threshold-linear network is guaranteed to converge to an equilibrium (which is dependent on the inputs and initial conditions) if and only if the matrix $\mathbf{I} - \mathbf{W}$ is copositive [72]. This condition is more general than the conditions provided for the matrix classes in Figure 6, as the set of P-matrices is a subset of the copositive matrices. While the copositivity condition provides a condition for convergence to an equilibrium, it does not guarantee the existence of multiattractiveness. The following result provides additional structural conditions on the synaptic weight matrix to guarantee multiattractiveness.

Theorem 4

(Conditional Multiattractiveness in a Brain Network [72]): Consider a threshold-linear brain network defined by symmetric synaptic weight matrix $\mathbf{W}$. If $\mathbf{I} - \mathbf{W}$ is copositive the following statements are equivalent:

1) The matrix $\mathbf{I} - \mathbf{W}$ is not positive semidefinite.
2) There exists a forbidden set.
3) The network is conditionally multiattractive.

This result can be interpreted as follows. The goal of the result is to provide conditions such that the network is conditionally multiattractive, and as such can encode multiple memories. By the first assumption in the result, that the matrix $\mathbf{I} - \mathbf{W}$ is copositive, we are guaranteed that for all inputs and initial conditions the dynamics converges to an equilibrium. From Theorem 4i) we get that a negative eigenvalue, which prevents the equilibrium point corresponding to all neurons being active from being stable, guaranteeing the forbidden set. This negative eigenvalue then allows for guaranteeing the conditional multiattractiveness of the network, as it allows for the construction of a separating hyperplane between stable equilibrium points guaranteed by the copositivity of $\mathbf{I} - \mathbf{W}$, giving disconnected equilibrium points, and the ability to encode multiple memories in the network.

We finish this section with a discussion of some of the additional assumptions we have added in this section. First, we have used the non-saturating threshold-linear model rather than the linear-threshold model. While being slightly less accurate, if it is assumed that the brain activity being considered is not approaching the saturation threshold, then the two models (bounded and unbounded) become equivalent. The use of this model is due to the requirement of input independence with memories defined in the manner of stable equilibrium points. If instead

we used the saturating model, then for any desired support we could construct a stable equilibrium by choosing an input that is sufficiently large in the active neurons and sufficiently negative in the inactive neurons to give an equilibrium point at the saturation threshold and zero. Since this is unrealistic, it motivates the use of threshold-linear models. Second, we have made the assumption that the synaptic weight matrix is symmetric, which then does not generally satisfy Dale's Law (except in cases where all neuron populations are excitatory or inhibitory). This assumption simplifies the analysis for multiple equilibrium points, but can prevent the existence of behavior such as oscillations [26]. However, under assumptions of a recurrently connected network and having fast-acting inhibitory neurons, the symmetric model can typically be a valid approximation [72].

Permitted Memories in Threshold-Linear Networks

In the prior section we provided conditions such that a network has the ability to encode and retrieve multiple memories. However, it is of interest to be able to determine whether the network structure permits the encoding of a memory in a given set of nodes. As such we are interested in determining if a given set of nodes is permitted or forbidden. The piecewise-affine nature of the threshold-linear dynamics and the relation between permitted sets and stable equilibrium points motivates the following result for determining if a set is permitted or forbidden.

Theorem 5

(Conditions for Permitted and Forbidden Sets [73]): Consider a threshold-linear network (13) with synaptic weight matrix $\mathbf{W}$. A set $\sigma \subseteq \{1,\dots,n\}$ is permitted if and only if the matrix $(-\mathbf{I}+\mathbf{W})_\sigma$, the principal submatrix corresponding with the indices in σ, is stable. Further, the set σ is forbidden if and only if $(-\mathbf{I}+\mathbf{W})_\sigma$ is unstable.

This result gives a simple test for whether or not a set of neurons allows for the encoding of a memory. It follows from the fact that each possible memory (and hence support) corresponds with an individual switching region in the threshold-linear dynamics. The existence of a stable equilibrium point with that support can then be determined using the same conditions as for a standard linear system, that is the stability of the synaptic weight matrix.

It is important to note that unlike the results in the prior section on multiattractiveness, this result does not require the synaptic weight matrix to be symmetric nor $\mathbf{I}-\mathbf{W}$ to be copositive. However, due to these omissions, it does not directly apply with Theorem 4, in that the existence of a forbidden set does not imply conditional multiattractiveness. If we do enforce those conditions again we obtain the following result.

Corollary 1

(Set Operations on Permitted and Forbidden Sets [72]): Consider a threshold-linear (13) brain network with symmetric synaptic weight matrix $\mathbf{W}$ such that $\mathbf{I}-\mathbf{W}$ is copositive. Then all subsets of permitted sets are permitted and all supersets of forbidden sets are forbidden.

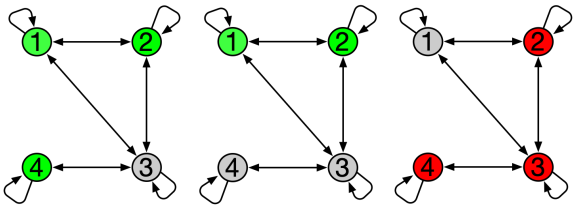

FIGURE 9 The network (14) with two permitted sets and one forbidden set highlighted. We see that a memory can be encoded on the set $\{1,2,4\}$ and no memories can be encoded on the set $\{2,3,4\}$ from the first and third images, respectively. The middle image illustrates that a memory can be encoded on the node set $\{1,2\}$, which can be determined both by Theorem 5 and by Corollary 1.

This result gives a way to determine a variety of permitted and forbidden sets based off the knowledge of just one permitted (or forbidden) set. In concert with Theorem 5, it makes it possible to determine many permitted or forbidden sets with minimal computations on the stability of matrices. In particular, by determining small forbidden sets, which requires minimal computational power, node sets can be ruled out immediately when looking for larger permitted sets, which requires more computational power due to considering larger matrices. The opposite use of this result is that if a single permitted set is found, then a large number can be constructed using subsets of the original set.

We finish this section with an example of a network able to encode multiple memories. Consider a threshold-linear brain network with four nodes and symmetric weight matrix $\mathbf{W}$ given by

$$\mathbf{W} = \begin{bmatrix} 0.8 & 0.2 & -0.5 & 0 \\ 0.2 & 0.3 & -0.2 & 0 \\ -0.5 & -0.2 & 0.4 & -0.4 \\ 0 & 0 & -0.4 & 0.9 \end{bmatrix}. \tag{14}$$

This matrix satisfies $\mathbf{I}-\mathbf{W}$ copositive, while also satisfying that it is not positive semidefinite. As such, by Theorem 4 there exists a forbidden set and the network can encode multiple memories. In Figure 9 we show the network with two permitted and one forbidden set highlighted, as determined by the conditions in Theorem 5. Using Corollary 1 we can determine that all subsets of $\{1,2,4\}$ are able to encode memories, while all supersets of $\{2,3\}$ are unable to encode memories.

From this example and following from Corollary 1, we see that permitted sets resulting from different inputs can contain some of the same neurons, or overlap. This corresponds with the idea of mixed selectivity, which is the idea of individual neurons responding to multiple, statistically independent variables [74]. As mixed selectivity has been shown to be important for performance in complex cognitive tasks, including memory [75], the ability to demonstrate this phenomenon is an advantage of the model.

ANALYSIS OF INTERCONNECTED BRAIN REGIONS

While studying the brain using models of individual brain regions can be useful, one of the defining characteristics of the brain is its interconnected structure between regions that can have vastly different properties. Almost all brain functions are based on the interaction and transmission of information between different areas, with other actions performed through the transmission of information into other parts of the nervous system. As such it is of interest to expand our study to models composed of multiple brain regions. We maintain the model of linear-threshold firing rate dynamics for each region and connect them to create larger networks of networks, as described in "Construction of Multi-Region Brain Networks". These networks can be formed with a variety of different topologies which appear based on network location and application.

In this section, we will expand our treatment of both GDSA and epileptic seizures to interconnected brain networks. For GDSA we will consider two network topologies, hierarchical thalamocortical networks and star-connected thalamocortical networks, and illustrate that selective inhibition and recruitment can be achieved in the interconnected networks based on properties of the linear-threshold dynamics. For modeling epileptic seizures, we will consider networks composed of interconnected excitatory-inhibitory pairs, and examine how oscillations occur and spread throughout the network governed by linear-threshold dynamics.

GDSA in Interconnected Brain Networks

Goal-driven selective attention occurs based on interactions and the transmission of information between areas in the brain. Here, we expand our treatment of selective inhibition and recruitment to networks composed of multiple brain regions. A key part of interconnected networks is that brain regions are not necessarily homogeneous and, as such, it is important to consider types with different characteristics. In particular, we consider networks composed of both cortical and thalamic regions and, using the construction of interconnected linear-threshold brain networks from "Construction of Multi-Region Brain Networks", will examine the following topologies:

- A *hierarchical thalamocortical topology*, as shown in Figure 10(a). In this topology, we consider a series of cortical regions forming a hierarchy, where each region is connected only to regions directly above and below. The thalamus is represented by a single region, composed of multiple higher-order thalamic nuclei, which accepts inputs from cortical regions, before modulating them and transmitting the information back to other cortical regions. This models transthalamic pathways that function parallel to the direct cortico-cortical connections [46]. By connecting to each cortical region in the hierarchy, this topology allows for the indirect connection of any two cortical regions through the thalamus. Such a topology has been implicated in higher-level brain functions, such as learning and decision-making, where the thalamus supports the transfer of information across different areas of the prefrontal cortex [76].
- A *star-connected thalamocortical topology*, as shown in Figure 10(b). In this topology, the thalamus node is a first-order thalamic nuclei, which transmits sensory or other information from subcortical structures to cortical regions. Here the thalamus is operating mostly as a relay. Such topologies arise in all sensory systems, with the exception of the olfactory system. Examples of first-order thalamic nuclei that result in this topology are the ventral posterior nucleus in the somatosensory system and the lateral geniculate nucleus in the visual system [77], [78].

Achieving selective inhibition and recruitment is dependent on the stabilizability of the network. When considering an interconnected network, the stabilizability of the overall network is dependent on the network timescales and interconnections, in addition to the internal dynamics of each region. As such, the results using direct feedback and feedforward inhibition in order to achieve selective recruitment and inhibition, Theorems 1 and 2, are not directly applicable. However, properties of the linear-threshold dynamics can be used to show that selective inhibition and recruitment is possible in the interconnected networks of both topologies, as discussed next.

Hierarchical Networks

The brain has been known to have a hierarchical organization for decades, both in terms of structure and function [79], [80]. One of these hierarchies is based upon function, in which primary sensory and motor areas are placed at the bottom of the hierarchy, while high-level processing areas such as the prefrontal cortex lie at the top [81]. Sensory information is processed as it moves up the hierarchy, while decisions are made at the top and information is then transmitted back down the hierarchy to perform desired actions or shape sensory perception. It is in the top-down direction of this hierarchy that GDSA occurs, where the higher-level layers instruct the lower layers as to which information is relevant, thus requiring further processing for performing the desired actions, and which information should be suppressed and prevented from further processing.

In addition to being sorted based upon the direction of information flow, a hierarchy of timescales also exists between brain regions, which closely aligns with the former. In particular, as one moves up the hierarchy, the regional dynamics become slower [82], [83], [44]. This separation of timescales is important for the ability of the network to perform selective inhibition and recruitment. To illustrate this, recall that the goal of GDSA is to have the activation level of the task-irrelevant components of the network converge to zero, while the activation level of the task-relevant components converge to a desired (non-zero) steady-state pattern, such as an equilibrium $\mathbf{x}^*$. In the case of a network of networks, the determination of such equilibria at each layer is not trivial, as the layer interconnection makes it dependent upon the inputs of layers higher in the hierarchy. The timescale separation plays a key role in reasoning about such

CONSTRUCTION OF MULTI-REGION BRAIN NETWORKS

Multi-region brain networks are constructed through the interconnection of the dynamics of individual brain regions. This occurs through the definition of sensory information processing pathways along connections within the structure of the network. Consider a single brain region, denoted by $\mathcal{N}_1$, and defined by the dynamics

$$\tau_1 \dot{\mathbf{x}}_1 = -\mathbf{x}_1 + [\mathbf{W}_{1,1}\mathbf{x}_1 + \mathbf{d}_1(t)]_{\mathbf{0}}^{\mathbf{m}_1}.$$

With the internal dynamics of the brain region given by the synaptic weight matrix $\mathbf{W}_{1,1}$, we define the processing pathways between regions in the input term $\mathbf{d}_1(t)$. Let $\mathcal{N}_2$ denote a second brain region, which we assume is connected to $\mathcal{N}_1$, forming a small network motif. Then, synaptic weight matrices $\mathbf{W}_{1,2}$ and $\mathbf{W}_{2,1}$ represent the information processing pathways between the two regions, defining the structure of the overall network. The input term $\mathbf{d}_1(t)$ for $\mathcal{N}_1$ is then given by

$$\mathbf{d}_1(t) = \mathbf{W}_{1,2}\mathbf{x}_2 + \mathbf{B}_1\mathbf{u}_1(t) + \mathbf{c}_1,$$

where $\mathbf{u}_1(t)$ is the control term for the region, and $\mathbf{c}_1$ corresponds to nonzero bias terms and any unmodeled background activity. Then, defining the dynamics of $\mathcal{N}_2$ with the same linear-threshold activation function, and defining $\mathbf{d}_2(t)$ analogously, the dynamics for the overall network composed of $\mathcal{N}_1$ and $\mathcal{N}_2$ is

$$\begin{aligned}\tau_1 \dot{\mathbf{x}}_1 &= -\mathbf{x}_1 + [\mathbf{W}_{1,1}\mathbf{x}_1 + \mathbf{W}_{1,2}\mathbf{x}_2 + \mathbf{B}_1\mathbf{u}_1(t) + \mathbf{c}_1]_{\mathbf{0}}^{\mathbf{m}_1}\\ \tau_2 \dot{\mathbf{x}}_2 &= -\mathbf{x}_2 + [\mathbf{W}_{2,2}\mathbf{x}_2 + \mathbf{W}_{2,1}\mathbf{x}_1 + \mathbf{B}_2\mathbf{u}_2(t) + \mathbf{c}_2]_{\mathbf{0}}^{\mathbf{m}_2}.\end{aligned}$$

This process can then be used iteratively to construct brain networks of arbitrary size and connectivity structure, which we will subsequently use to study GDSA and epileptic seizures over interconnected brain networks.

equilibria. This is because, for a given layer, the state of the ones above it can be considered as constant (since they evolve on a slower time scale), whereas the state of the ones below it can be described as a static nonlinear function dependent upon the state of the current layer (since they evolve on a faster time scale).

Formally, one defines an equilibrium map, which we denote $h_i^1(\cdot)$ (where the superindex 1 indicates that this is for the task-relevant nodes), for each layer i. This map, given the inputs from the higher layers in the network, returns the set of equilibria for network layer i. One can set the state of the task-irrelevant nodes to zero (as this will be taken care of by selective inhibition) and shrink the state of each layer to strictly include the task-relevant components. The equilibrium maps require a constant input representing the state of the layers higher in the network, whose existence can be justified through the timescale separation between layers in the hierarchical network and using singular perturbation theory. Under the assumption that the timescale separation is infinitely large, and assuming global asymptotic stability of each layer, the state of a given layer appears as a constant at the timescale of the lower layers in the hierarchy. Conversely, at the timescale of layers above, the state of a lower layer becomes a static nonlinear function (the equilibrium map) of the states of the higher layers of the hierarchy. Utilizing this, the equilibrium map takes its inputs to be the state (modified through interconnection matrices) of any layers higher in the network that are directly connected. In the hierarchical thalamocortical topology this is either one or two inputs. The first input is the cortical layer directly above the considered layer. Then, if the current layer is below the thalamus in the hierarchy, the state of the thalamus will also be an input to the equilibrium map. We are then able to recursively define equilibrium maps from the bottom layer up to the top of the hierarchy.

Utilizing these equilibrium maps, and the goal equilibrium they define for selective recruitment, we next discuss conditions for achieving selective inhibition and recruitment in the cortical and thalamocortical hierarchical networks. The hierarchical thalamocortical network, shown in Figure 10(a), is composed of N cortical regions connected to the regions directly above and below and one thalamic region connected to all of the cortical regions. In order to represent the thalamus as a single region we assume that the relevant thalamic neurons have comparable timescales. The regions form a temporal (and functional) hierarchy, encoded by timescales satisfying $\tau_1 \gg \tau_2 \gg \cdots \gg \tau_N$. The thalamus region, forming parallel transthalamic pathways lies in the same hierarchy. The exact position of the thalamus is dependent on the cortical regions in the hierarchy, but it can lie at any point [84]. Without loss of generality we assume the thalamus lies at a point in the middle of the hierarchy, with $\tau_a \gg \tau_T \gg \tau_{a+1}$ for some $a \in \{1,\dots,N\}$. The results that follow remain valid if the thalamus is at an endpoint (top or bottom) of the hierarchy, with slight changes in the resulting expressions. Using the linear-threshold firing rate model (3), we obtain the following dynamics for the hierarchical network,

$$\begin{aligned}\tau_i \dot{\mathbf{x}}_i &= -\mathbf{x}_i + [\mathbf{W}_{i,i}\mathbf{x}_i(t) + \mathbf{W}_{i,i-1}\mathbf{x}_{i-1}(t) + \mathbf{W}_{i,i+1}\mathbf{x}_{i+1}(t)\\ &\qquad + \mathbf{W}_{i,T}\mathbf{x}_T + \mathbf{B}_i\mathbf{u}_i(t) + \mathbf{c}_i)]_{\mathbf{0}}^{\mathbf{m}_i}, \quad i \in \{1,\dots,N\}\\ \tau_T \dot{\mathbf{x}}_T &= -\mathbf{x}_T + [\mathbf{W}_T\mathbf{x}_T + \sum_{i=1}^{N} \mathbf{W}_{T,i}\mathbf{x}_i + \mathbf{B}_T\mathbf{u}_T(t) + \mathbf{c}_T]_{\mathbf{0}}^{\mathbf{m}_T}.\end{aligned} \tag{15}$$

From this dynamics we can define equilibrium maps for each layer in the cortical hierarchy, each giving the set of possible equilibrium points as a function of the constant $\mathbf{c}$. Note that these equilibrium maps are for the task-relevant portion of the dynamics only and, as such, are not impacted by the control input which acts only on the task-irrelevant components. Due to the interconnected form of the dynamics, the maps are defined recursively, with expressions dependent on the location of the region in the hierarchy. For the bottom layer of the network, the

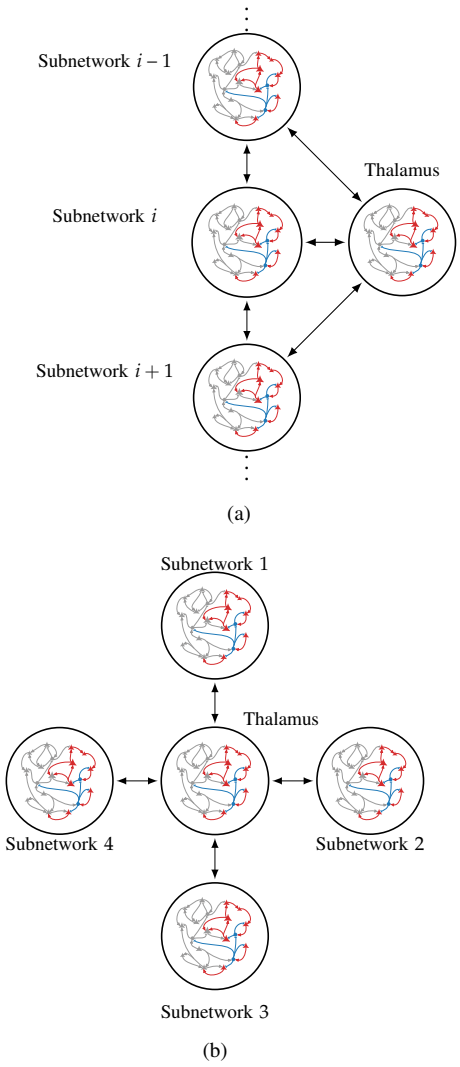

FIGURE 10 Topologies for thalamocortical multi-region brain networks considered in the paper: (a) multilayer hierarchical thalamocortical network, where each layer is connected directly to the thalamus, as well as the layers directly above and below it; (b) star-connected thalamocortical network, where each cortical layer is connected to the thalamus layer only. In both plots, task-relevant excitatory and inhibitory nodes are depicted in red and blue, respectively, and (transiently silenced) task-irrelevant nodes are depicted in grey.

equilibrium map is defined as

$$h_N^1(\mathbf{c}) = \{\mathbf{x}_N^1 \mid \mathbf{x}_N^1 = [\mathbf{W}_{N,N}^{11}\mathbf{x}_N^1 + \mathbf{c}]_{\mathbf{0}}^{\mathbf{m}_N^1}\}. \tag{16}$$

The equilibrium maps further up the hierarchy become notationally more complicated due to their recursive nature, but all maintain the form

$$h_i^1(\mathbf{c}) = \{\mathbf{x}_i^1 \mid \mathbf{x}_i^1 = [\mathbf{W}_{i,i}^{11}\mathbf{x}_i^1 + \sum_{j=i+1,T} \mathbf{W}_{i,j}^{11} h_j^1(\mathbf{y}) + \mathbf{c}]_{\mathbf{0}}^{\mathbf{m}_i^1}\}, \tag{17}$$

where, for an arbitrary layer i, the sum is over the layers below the current layer that are directly connected, potentially including the thalamus. Here $\mathbf{y}$ is an input into the equilibrium maps below layer i dependent on the state of the higher layers in the network. In these maps, the impact from the layers higher in the hierarchy on the current layer's equilibrium appear in the input term $\mathbf{c}$, while the impact from the lower networks comes from the appearance of the lower-level equilibrium maps.

The equilibrium maps can be written in a switched-affine form, denoted by

$$h_i^1(\mathbf{c}) = \mathbf{F}_\lambda \mathbf{c} + \mathbf{f}_\lambda$$

for switching regions λ, based on the piecewise-affine form of the linear-threshold dynamics (details on this form can be found in [7]). This representation of the equilibrium map gives rise to a gain matrix $\bar{\mathbf{F}}_i$, defined as the entry-wise maximum of the matrix $|\mathbf{F}_\lambda|$ over all switching regions. These gain matrices are relevant to the results providing conditions for selective inhibition and recruitment to be achieved in the interconnected network, as given next.

Theorem 6

(Selective Inhibition and Recruitment in Hierarchical Thalamocortical Networks [85]): Consider a thalamocortical hierarchical network governed by a linear-threshold dynamics and suppose subnetwork $\mathcal{N}_1$ has bounded trajectories. If

$$\rho(|\mathbf{W}_{i,i}^{11}| + |\mathbf{W}_{i,i+1}^{11}|\bar{\mathbf{F}}_{i+1}|\mathbf{W}_{i+1,i}^{11}|) < 1,$$

for layers below the thalamus,

$$\rho(|\mathbf{W}_{i,i}^{11}| + |\mathbf{W}_{i,i+1}^{11}|\bar{\mathbf{F}}_{i+1}|\mathbf{W}_{i+1,i}^{11}| + |\mathbf{W}_{i,T}^{11}|\bar{\mathbf{F}}_T|\mathbf{W}_T^{11}|) < 1,$$

for layers above the thalamus, and

$$\rho(|\mathbf{W}_T^{11} + \sum_{i=a+1}^{N} |\mathbf{W}_{T,i}^{11}|\bar{\mathbf{F}}_i|\mathbf{W}_{i,i}^{11}|) < 1,$$

then there exists $\mathbf{K}_i$ and $\bar{\mathbf{u}}_i(t)$ such that using the feedback-feedforward control $\mathbf{u}_i(t) = \mathbf{K}_i\mathbf{x}_i(t) + \bar{\mathbf{u}}_i(t)$, for all i, gives

$$\begin{cases} \mathbf{x}_i^0(t) \to \mathbf{0} & \text{for all } i \in \{2,\dots,N,T\} \\ \mathbf{x}_i^1(t) \to h_i^1(\mathbf{W}_{i,i-1}^{11}\mathbf{x}_{i-1}^1(t) + \mathbf{c}_i^1) & \text{for layers above the thalamus} \\ \mathbf{x}_i^1(t) \to h_i^1(\mathbf{W}_{i,i-1}^{11}\mathbf{x}_{i-1}^1(t) + \mathbf{W}_{i,T}^{11}\mathbf{x}_T^1(t) + \mathbf{c}_i^1) & \text{for layers below the thalamus} \\ \mathbf{x}_T^1(t) \to h_T(\sum_{i=1}^{a} \mathbf{W}_{T,i}^{11}\mathbf{x}_i^1(t) + \mathbf{c}_T). & \text{for the thalamus} \end{cases}$$

as the timescales satisfy $\frac{\tau_i}{\tau_{i-1}} \to 0$ and $\frac{\tau_T}{\tau_{a+1}} \to 0$ for all $i \in \{2,\dots,N\}$.

This result can be interpreted as follows. The conditions involving the spectral radius at each layer involve two components: the internal dynamics of layer $\mathcal{N}_i$, and the impact of its interconnections with the next layer in the hierarchy ($\mathcal{N}_{i+1}$) and the thalamus. Due to the timescale separation between layers in the hierarchy, the connections from the next layer in the hierarchy and the thalamus act as static nonlinearities due to their continual "instantaneous" convergence to their respective (and moving) equilibrium points. Therefore, the sums combine the pathways that $\mathcal{N}_i$ has to impact its state, and the spectral radius condition gives an upper bound on the combined effects of these pathways. If the spectral radius conditions hold, reduced-order dynamics for the task-relevant components in the

network constructed by replacing connections from lower layers in the hierarchy with their equilibrium values are GES [85, Lemma IV.2], which allows for the convergence to the desired equilibrium for GDSA. The result $\mathbf{x}_i^0(t) \to \mathbf{0}$ shows the task-irrelevant components of the dynamics converging to zero, with the remaining terms give convergence to a steady state, as expected. The control $\mathbf{u}_i(t)$ used to achieve this convergence is a feedback-feedforward control where each component plays a different role. The feedback term $\mathbf{K}_i\mathbf{x}_i$ is used to manage the impact of the layers of the network below layer i, while the feedforward term $\bar{\mathbf{u}}_i(t)$ controls the inputs from higher in the network and the term $\mathbf{c}_i^0$. Meanwhile, the value of the steady state the task-relevant components converge to is dependent on the terms $\mathbf{c}_1^1, \ldots, \mathbf{c}_N^1, \mathbf{c}_T^1$ and the interconnection between the network layers. In general it is difficult to specify values such that the network converges to a specific steady state, but this problem has been approached with a reservoir computing approach [86].

We now give some intuition on the remaining components of Theorem 6. First, the gain matrices $\bar{\mathbf{F}}_i$ provide a worst-case bound on how much the equilibrium point of a layer $\mathcal{N}_i$ can change based on one unit of change in the state of layer $\mathcal{N}_{i-1}$. Due to this, its use in the spectral radius conditions covering pathways for modifying system states makes the bound conservative. Second, the condition $\tau_i/\tau_{i-1} \to \mathbf{0}$ corresponds to the timescale separation between the layers becoming infinitely large. This separation, creating completely distinct timescales between each layer, provides the base for being able to apply a generalized Tikhonov-style singular perturbation argument [87] and establish the stabilizability of the hierarchical interconnected linear-threshold network. It is important to note that, while the result calls for an infinite timescale separation, in brain pathways the ratios between successive layers can be on the order of $1/1.5 \sim 1/2.5$, which we have empirically found to typically be sufficient for selectively inhibiting and recruiting the system with a small degree of tracking error [7]. In addition, note that the conditions of Theorem 6 for the stabilizability of interconnected linear-threshold networks, illustrated through the ability to achieve selective inhibition and recruitment, depend only on matrices of size $\mathbb{R}^{n_i \times n_i}$, where n_i is the size of layer $\mathcal{N}_i$. This corresponds with the analysis of the result occurring at the level of individual regions with the infinite timescale separation. The other method for analysis of the network is considering it as one large network with finitely different timescales. Taking this approach then leads to determining if selective inhibition and recruitment is possible through a calculation related to the full matrix of the network. In this case, if selective inhibition is not possible, we are not able to pinpoint where the problem in the network might be. As such it is preferable to take the approach of Theorem 6 as it provides greater interpretability by being able to determine smaller regions of the network that result in not being able to achieve selective inhibition and recruitment. In addition, in Theorem 6 we provide conditions based on the spectral radius of relevant matrices, which is efficient to calculate but conservative. In [85] more general conditions are provided which involve determining whether matrices are $\mathcal{L}$-matrices or totally Hurwitz. These conditions are much more difficult to confirm for larger matrices, providing further incentive for the hierarchical approach used here.

Finally, we note that, while the results in this section are technical, they have been used to connect linear-threshold networks with experimental neural data. For example, [7] uses the hierarchical linear-threshold model for a case study modeling selective listening in rats based on measurements of single-neuron activity in the prefrontal cortex and the primary auditory cortex.

Star-Connected Networks

A star-connected network, as shown in Figure 10(b), arises when we model the thalamus as a relay center, as is common in the studies of sensory processing [46], [88], [89]. In this context, the thalamus often receives an input signal from a subcortical area and sends outputs to one or more cortical regions. In this simplified model, the cortical regions are not directly connected and, hence, their timescale differences do not play an important role.

We model the (subcortical) region that provides the input to the thalamus with a linear-threshold firing rate model in the same manner as the other regions in the network, except for an explicit control term modeling the sensory input to the region and represented by a time-varying input signal $\mathbf{c}_1(t)$. Accordingly, we model the dynamics for a star-connected thalamocortical network with $N-1$ cortical regions as

$$\begin{aligned}
\tau_1\dot{\mathbf{x}}_1 &= -\mathbf{x}_1 + [\mathbf{W}_{1,1}\mathbf{x}_1 + \mathbf{W}_{1,T}\mathbf{x}_T + \mathbf{c}_1(t)]_{\mathbf{0}}^{\mathbf{m}_1} \\
\tau_i\dot{\mathbf{x}}_i &= -\mathbf{x}_i + [\mathbf{W}_{i,i}\mathbf{x}_i + \mathbf{W}_{i,T}\mathbf{x}_T + \mathbf{B}_i\mathbf{u}_i + \mathbf{c}_i]_{\mathbf{0}}^{\mathbf{m}_i} \\
\tau_T\dot{\mathbf{x}}_T &= -\mathbf{x}_T + [\mathbf{W}_T\mathbf{x}_T + \sum_{i=1}^{N}\mathbf{W}_{T,i}\mathbf{x}_i + \mathbf{B}_T\mathbf{u}_T + \mathbf{c}_T]_{\mathbf{0}}^{\mathbf{m}_T}, \quad (18)
\end{aligned}$$

where $i \in \{2, \ldots, N\}$, $\mathbf{x}_1$ denotes the state vector of the subcortical region providing sensory input to the thalamus and the terms $\mathbf{c}_2, \ldots, \mathbf{c}_N, \mathbf{c}_T$ are unmodeled background activity that also shape the desired steady-state convergence point.

Due to the lack of temporal hierarchy in this network topology, the singular perturbation method used earlier for the hierarchical architectures no longer applies. First, with the lack of timescale separation, the equilibrium of the network is no longer determined through recursive equilibrium maps and, instead, must be computed concurrently for all subnetworks. In particular, the network equilibrium at time t is given by the solution to the following set of nonlinear equations

$$\begin{aligned}
\mathbf{x}_1^1 &= [\mathbf{W}_{1,1}^{1,\text{all}}\mathbf{x}_1 + \mathbf{W}_{1,T}^{1,\text{all}}\mathbf{x}_T + \mathbf{c}_1^1(t)]_{\mathbf{0}}^{\mathbf{m}_i^1}, \\
\mathbf{x}_i^1 &= [\mathbf{W}_{i,i}^{1,\text{all}}\mathbf{x}_i + \mathbf{W}_{i,T}^{1,\text{all}}\mathbf{x}_T + \mathbf{c}_i^1]_{\mathbf{0}}^{\mathbf{m}_i^1}, \qquad i = 2, \ldots, N, \\
\mathbf{x}_T^1 &= [\mathbf{W}_T\mathbf{x}_T + \sum_{i=1}^{N}\mathbf{W}_{T,i}\mathbf{x}_i + \mathbf{c}_T^1]_0^{\mathbf{m}_T^1},
\end{aligned}$$

where $\mathbf{x}_i^0 = \mathbf{0}$ for all $i \in \{1, \ldots, N, T\}$. For considering selective inhibition and recruitment in the star-connected topology, we

instead use results on the stability of slowly varying nonlinear systems. These rely on assuming that the input signal to the subcortical region, $\mathbf{c}_1(t)$, has a bounded-rate derivative (that is, there exists finite α such that $\|\dot{\mathbf{c}}_1(t)\| < \alpha$). In addition, we allow for a slightly weaker notion of selective inhibition and recruitment in which the convergence to zero and the equilibrium, respectively, is within a constant ϵ. The following result provides conditions such that the thalamocortical network with a star-connected topology can achieve this notion of selective inhibition and recruitment.

Theorem 7

(Selective Inhibition and Recruitment in Star-Connected Thalamocortical Networks [85]): Consider an N-layer star-connected thalamocortical network with $N-1$ cortical regions $\mathcal{N}_2, \ldots, \mathcal{N}_N$, thalamic layer $\mathcal{N}_T$ and subcortical input layer $\mathcal{N}_1$. Suppose the following hold for all values of $\mathbf{c}_i \in \mathbb{R}^{n_i}$, $i \in \{2, \ldots, N\}$ and $\mathbf{c}_T \in \mathbb{R}^{n_T}$:

1) The input layer $\mathcal{N}_1$ has no nodes to be inhibited, $\rho(\mathbf{W}_{1,1}|) < 1$, and the input $\mathbf{c}_1(t)$ lies in a compact set and has a bounded rate derivative;
2) For each $i \in \{2, \ldots, N\} \cup \{T\}$, the matrix $\mathbf{W}^{11}_{i,i}$ satisfies $\rho(|\mathbf{W}^{11}_{i,i}) < \alpha_i$, with $\alpha_i < 1$;
3) The matrix of task-relevant interconnections

$$\bar{\mathbf{W}}^{11} = \begin{bmatrix} \mathbf{W}_{1,1} & \mathbf{0} & \ldots & \mathbf{0} & \mathbf{W}^{11}_{1,T} \\ \mathbf{0} & \mathbf{W}^{11}_{2,2} & \ldots & \mathbf{0} & \mathbf{W}^{11}_{2,T} \\ \vdots & \ldots & \ddots & \vdots & \vdots \\ \mathbf{0} & \mathbf{0} & \ldots & \mathbf{W}^{11}_{N,N} & \mathbf{W}^{11}_{N,T} \\ \mathbf{W}^{11}_{T,1} & \mathbf{W}^{11}_{T,2} & \ldots & \mathbf{W}^{11}_{T,N} & \mathbf{W}^{11}_{T} \end{bmatrix},$$

with Schur decomposition[1] $\bar{\mathbf{W}}^{11} = \mathbf{Q}^\top(\mathbf{D}_{\bar{\mathbf{W}}^{11}} + \mathbf{N}_{\bar{\mathbf{W}}^{11}})\mathbf{Q}$, is such $\alpha + \max(\delta, \delta^{1/p}) < 1$, where p is the dimension of $N_{\bar{\mathbf{W}}^{11}}$ and

$$\alpha = \max_{i \in \{2,\ldots,N\} \cup \{T\}} \{\alpha_i\}, \qquad \delta = \gamma \sum_{j=1}^{p-1} \|N_{\bar{\mathbf{W}}^{11}}\|^j$$

$$\gamma = \max\{\sum_{i=1}^{N-1} \mathbf{W}^{11}_{i,t}\mathbf{W}^{11^\top}_{i,T}, \sum_{i=1}^{N-1} \mathbf{W}^{11}_{T,i}\mathbf{W}^{11^\top}_{T,i}\}$$

Then there exist equilibrium maps $\mathbf{x}^*_i(t)$ and $\epsilon > 0$ such that

$$\begin{cases} \lim_{t\to\infty} \|\mathbf{x}_1(t) - \mathbf{x}^*_1(\mathbf{c}_1(t))\| < \epsilon \\ \qquad \text{(Selective Recruitment of Driving Layer)} \\ \text{and for all layers } \{\mathcal{N}_i\}_{i=2}^N \text{ and } \mathcal{N}_T, \\ \quad \lim_{t\to\infty} \|\mathbf{x}^0_i(t)\| < \epsilon; \\ \qquad \text{(Selective Inhibition)} \\ \quad \lim_{t\to\infty} \|\mathbf{x}^1_i(t) - \mathbf{x}^{1^*}_i(\mathbf{c}_1(t), \ldots, \mathbf{c}_N, \mathbf{c}_T)\| < \epsilon \\ \qquad \text{(Selective Recruitment)} \end{cases}$$

Further, if $\|\dot{\mathbf{c}}_1(t)\| \to 0$ as $t \to \infty$ then $\epsilon = 0$.

[1]For a matrix $\mathbf{W}$ we consider the Schur decomposition $\mathbf{W} = \mathbf{Q}^\top(\mathbf{D} + \mathbf{N})\mathbf{Q}$ where $\mathbf{Q}$ is unitary, $\mathbf{D}$ is diagonal, and $\mathbf{N}$ is upper triangular with a zero diagonal [90].

The result in Theorem 7 can be interpreted as follows: the star-connected network can achieve selective inhibition and recruitment if each layer of the network dynamics is independently stable and the magnitude of the thalamocortical and corticothalamic connections does not exceed a determined stability margin. This bound on the magnitude of the corticothalamic feedback in the network aligns with neuroscientific observations: it has been seen that enhanced corticothalamic feedback can result in pathological behavior [45]. In particular, strong corticothalamic feedback has been found to coincide with epileptic loss of consciousness in absence seizures due to over-inhibition of the cortical regions [91]. Star-connected thalamocortical networks have also been associated with other behavior seen in the brain, see for example "Remote Synchronization in Star-Connected Thalamocortical Networks".

Comparison of Selective Inhibition and Recruitment Across Interconnected Topologies

We have shown that the linear-threshold rate dynamics allow for the network to achieve selective inhibition and recruitment in multiple interconnected network topologies. In the two topologies considered, the thalamus serves significantly different roles: those of first order versus higher order nuclei [46]. This, in turn, results in different network properties across the two topologies, including different conditions for achieving selective inhibition. In particular, the hierarchical network is strongly dependent on the interconnection properties between the cortical regions, whereas the star-connected network is more reliant on the internal dynamics of each layer.

However, a star-connected topology can also arise directly from the hierarchical thalamocortical network in the case of damage to the network. If the hierarchical thalamocortical network incurs injury such that one or more of the information pathways between cortical regions are damaged, the network topology becomes locally akin to the star topology of Figure 10(b). This possibility underscores the importance of the transthalamic pathways between cortical regions and the ability to achieve selective inhibition and recruitment in a star-connected network. Indeed, if we consider a strictly cortical hierarchy as in [7], the removal of any information pathway would disconnect the underlying chain-like topology. In the following example, we illustrate achieving selective inhibition and recruitment in a hierarchical thalamocortical network along with the star-connected network formed by damage to the corticocortical connections.

We consider a hierarchical network composed of three cortical layers and one thalamic layer. Each layer is composed of three neurons, with the top layer being purely excitatory and the thalamus being purely inhibitory. The second layer is composed of two inhibitory nodes and one excitatory, while the third contains two excitatory and one inhibitory nodes. We drive the top layer with an oscillatory input and aim to selectively inhibit and recruit nodes in the remaining three layers. The parameters for the network are as follows.

REMOTE SYNCHRONIZATION IN STAR-CONNECTED THALAMOCORTICAL NETWORKS

A phenomenon of vast classical and recent interest in neuroscience is that of synchronization between brain regions [169], [170]. In particular, *remote synchronization* refers to the condition where regions in a network synchronize despite a lack of direct links between them [171]. Remote synchronization is frequently studied in networks of oscillators, such as the Kuramoto model [172] of neural population phase oscillators. In particular, [173] studies remote synchronization in star-connected networks where synchronization can only happen remotely between peripheral nodes due to the lack of direct connections between them.

Remote synchronization is also commonly observed in the brain between distant cortical regions, often in the context of functional connectivity analysis [174]. Given the thalamus' hub-like connectivity to cortical regions (similar to the above star topology), the thalamus has been suggested to play a key role in remote synchronization within the brain [175]. Interestingly, it is shown in [176] that remote synchronization is dependent on symmetry between the outer regions in a star-connected topology, a phenomenon that is also shown to hold for remote synchronization of both linear-threshold and Kuramoto oscillator star-connected thalamocortical networks in [85] and [173], respectively.

$$\mathbf{W}_1 = \begin{bmatrix} 0.4461 & 0.1125 & 0.4637 \\ 0.1213 & 0.1750 & 0.0257 \\ 0.0648 & 0.1435 & 0.2963 \end{bmatrix} \quad \mathbf{W}_2 = \begin{bmatrix} 0.4005 & -0.3816 & -0.3963 \\ 0.1165 & -0.4132 & -0.1645 \\ 0.4662 & -0.2867 & -0.1117 \end{bmatrix}$$

$$\mathbf{W}_{21} = \begin{bmatrix} 0.1668 & 0.3416 & 0.4702 \\ 0.1148 & 0.4811 & 0.0029 \\ 0.4681 & 0.2190 & 0.3052 \end{bmatrix} \quad \mathbf{W}_{12} = \begin{bmatrix} 0.0814 & -0.2511 & -0.0235 \\ 0.4192 & -0.4997 & -0.1068 \\ 0.0838 & -0.1777 & -0.1989 \end{bmatrix}$$

$$\mathbf{W}_{T,1} = \begin{bmatrix} 0.4782 & 0.1382 & 0.4817 \\ 0.2865 & 0.3112 & 0.0430 \\ 0.4249 & 0.2942 & 0.2502 \end{bmatrix} \quad \mathbf{W}_{32} = \begin{bmatrix} 0.4136 & -0.2379 & -0.4003 \\ 0.3379 & -0.1995 & -0.0525 \\ 0.1245 & -0.2997 & -0.4107 \end{bmatrix}$$

$$\mathbf{W}_T = \begin{bmatrix} -0.3482 & -0.4450 & -0.0570 \\ -0.2599 & -0.1651 & -0.1555 \\ -0.0295 & -0.1149 & -0.1142 \end{bmatrix} \quad \mathbf{W}_3 = \begin{bmatrix} 0.4205 & 0.2861 & -0.3789 \\ 0.1773 & 0.3504 & -0.1946 \\ 0.2150 & 0.3712 & -0.2147 \end{bmatrix}$$

$$\mathbf{W}_{1,T} = \begin{bmatrix} -0.1184 & -0.4869 & -0.4300 \\ -0.3511 & -0.4862 & -0.2009 \\ -0.1877 & -0.3218 & -0.3160 \end{bmatrix} \quad \mathbf{W}_{23} = \begin{bmatrix} 0.1562 & 0.1452 & -0.3074 \\ 0.2923 & 0.2013 & -0.4956 \\ 0.4150 & 0.4310 & -0.1018 \end{bmatrix}$$

$$\mathbf{W}_{2,T} = \begin{bmatrix} -0.4961 & -0.4507 & -0.0542 \\ -0.2012 & -0.4977 & -0.0181 \\ -0.3294 & -0.3266 & -0.3090 \end{bmatrix} \quad \mathbf{W}_{T,3} = \begin{bmatrix} 0.2228 & 0.1519 - 0.3992 \\ 0.4220 & 0.2416 - 0.4937 \\ 0.0981 & 0.1689 - 0.0795 \end{bmatrix}$$

$$\mathbf{W}_{T,2} = \begin{bmatrix} 0.2608 & -0.4422 & -0.0742 \\ 0.0451 & -0.2195 & -0.3099 \\ 0.4523 & -0.3909 & -0.1303 \end{bmatrix} \quad \mathbf{W}_{3,T} = \begin{bmatrix} -0.2836 & -0.3313 & -0.4810 \\ -0.4810 & -0.2617 & -0.2701 \\ -0.3731 & -0.1299 & -0.0151 \end{bmatrix}$$

$$\mathbf{c}_1 = \mathbf{c}_2 = \mathbf{c}_T = \begin{bmatrix} 0.5 \\ 1.25 \\ 2 \end{bmatrix} \quad \mathbf{c}_3 = \begin{bmatrix} 2 \\ 1.25 \\ 2 \end{bmatrix}$$

The threshold is set to be $\mathbf{m} = 10$ and timescales are $\tau_1 = 3$, $\tau_2 = 1.625$, $\tau_3 = 0.25$, and $\tau_T = 1$. These parameters satisfy the conditions of Theorem 6 and in Figure 11 we show that we can achieve selective inhibition and recruitment for the hierarchical network with the aim of inhibiting one node in each of the layers other than the top layer. The remaining nodes are recruited to oscillatory equilibrium trajectories based on the equilibrium maps (17). Note that they are non-constant trajectories since we drive the top layer in an oscillatory manner.

We next consider the scenario where the corticocortical connections in the network are severed, resulting in a star-connected network. Note that a hierarchy of timescales still remains between the layers. In Figure 12, we see that we can still achieve selective inhibition and recruitment, but the equilibrium trajectories to which the task-relevant nodes are recruited are different than the original network. This is expected as the equilibrium maps are dependent on the interconnections between the cortical regions, which are now all zero.

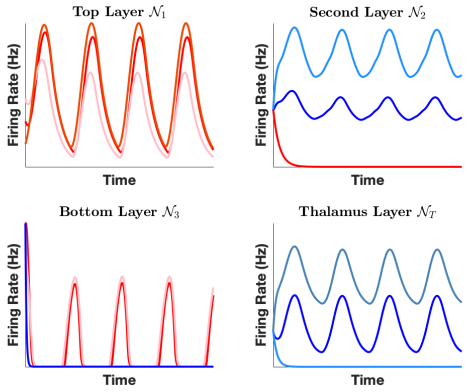

FIGURE 11 Selective inhibition in a three-layer hierarchical thalamocortical network. In the second, third, and thalamic layers, one node is selectively inhibited while the other two are recruited.

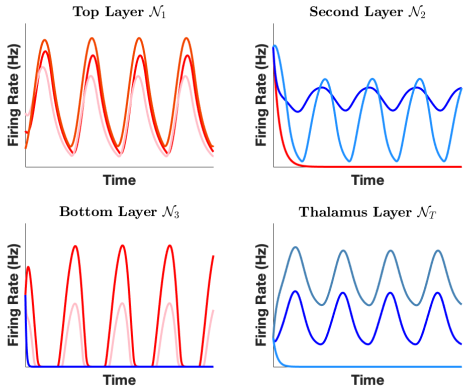

FIGURE 12 Selective inhibition in a three-layer star-connected thalamocortical network formed by removing the corticocortical connections from a hierarchical network. In the second, third, and thalamic layers, one node is selectively inhibited while the other two are recruited. As in the original network, selective inhibition and recruitment is achieved, but the recruitment is to a different set of equilibria trajectories, as expected.

This example illustrates that the linear-threshold dynamics are stabilizable in interconnected networks with conditions dependent on the topologies of the network. This matches the fact that different regions of the brain have different topologies but are still able to exhibit similar phenomena.

Epilepsy in Interconnected Linear-Threshold Networks

We have already analyzed the emergence of epileptic seizures through bifurcations, representing a sudden change from healthy to unhealthy dynamics, in the linear-threshold model for a single brain region. However, more complex patterns emerge during an epileptic seizure when looking at networks of multiple brain regions. One such pattern is the excessive synchrony of activity between regions. Further, recalling from Remark 1 that different oscillatory waveforms in the EEG are observed during seizures [92], [93], epileptic behavior can appear when there are extensive synchronous oscillations throughout the brain [94]. It has been suggested that the *broad spread* of synchronized pathological oscillations is a critical factor in generalized seizures [95], whereas hyper-synchronized oscillations confined to a local brain area do not necessarily give rise to a seizure [96]. In the following, we discuss epileptic behavior through the modeling of oscillation spreading throughout an interconnected network of excitatory-inhibitory pairs in a synchronous manner, following the exposition in [97]. We study excitatory-inhibitory pairs as they are simple but non-trivial networks that exhibit rich dynamical behavior, and allow for the construction of large high-dimensional systems through the interconnection of many pairs. In this section we consider coupled networks of E-I pairs which are defined by the interconnection of the dynamics of individual E-I pairs, modeling information processing pathways between regions. We construct a network of N coupled E-I pairs as follows. Each E-I pair has dynamics defined by synaptic weight matrix $\mathbf{W}_i$, input $\mathbf{u}_i$ and threshold $\mathbf{m}_i$:

$$\mathbf{W}_i = \begin{bmatrix} a_i & -b_i \\ c_i & -d_i \end{bmatrix} \qquad \mathbf{u}_i = \begin{bmatrix} u_i^E \\ u_i^I \end{bmatrix} \qquad \mathbf{m}_i = \begin{bmatrix} m_i^E \\ m_i^I \end{bmatrix}.$$

The coupling between E-I pairs i and j is then defined by weight matrix $\mathbf{W}_{ij}$ of the form

$$\mathbf{W}_{ij} = \begin{bmatrix} w_{ij}^{EE} & -w_{ij}^{EI} \\ w_{ij}^{IE} & -w_{ij}^{II} \end{bmatrix}.$$

The weights $w_{ij}^{EE}, w_{ij}^{EI}, w_{ij}^{IE}$ and w_{ij}^{II} are nonnegative values that define the excitatory-excitatory, excitatory-inhibitory, inhibitory-excitatory and inhibitory-inhibitory connections, respectively. Then, the coupled E-I pair network has dynamics for the excitatory and inhibitory components of node i given by

$$\begin{aligned} \dot{x}_i^E &= -x_i^E + [a_i x_i^E - b_i x_i^I + \sum_{j \neq i} (w_{ij}^{EE} x_j^E + w_{ij}^{EI} x_j^I) + u_i^E]_0^{m_i^E} \\ \dot{x}_i^I &= -x_i^I + [c_i x_i^E - d_i x_i^I + \sum_{j \neq i} (w_{ij}^{IE} x_j^E + w_{ij}^{II} x_j^I) + u_i^I]_0^{m_i^I}. \end{aligned} \tag{19a}$$

This notation for networks of coupled excitatory-inhibitory pairs will be used in studying oscillation spreading through these networks in the context of epilepsy.

As oscillations are a key part of the modeling of epileptic seizures in this approach, we first discuss conditions such that oscillations appear in individual linear-threshold networks, before considering their synchronization and spreading between interconnected regions.

Oscillations in Linear-Threshold Networks

Oscillations can arise in linear-threshold brain networks under a variety of conditions. Instead of using perfectly periodic trajectories (as in a limit cycle) as the defining property of an oscillatory system, we use lack of stable equilibria. This choice is motivated by the hypotheses in the Poincaré-Bendixson theorem [98] for establishing the existence of limit cycles in planar systems, but (1) relaxes the (unrealistic) need for exact periodicity and allows for chaotic oscillations that better match biological neural oscillations, and (2) opens the door to theoretical analyses in higher-dimensional systems. As such, we put forth the following definition of oscillatory behavior.

Definition 8

(Oscillatory and Inactive Nodes [97]): Consider a linear-threshold network (3) composed of n nodes. We say that the ith node of the system is *oscillatory* if for all solutions of network dynamics, $\mathbf{x}_i(t)$ does not converge to a constant value as $t \to \infty$. Furthermore, a non-oscillatory node is said to be *inactive* if for all network solutions, $\mathbf{x}_i(t) \to 0$ as $t \to \infty$.

As noted earlier, we are interested in the spreading of oscillations in networks of interconnected excitatory-inhibitory pairs. This begins by investigating the appearance of oscillations in an individual excitatory-inhibitory pair. For that, consider the linear-threshold dynamics (3) with constant input $\mathbf{u}(t) = \mathbf{u}$ for all $t \in \mathbb{R}$ and synaptic weight matrix

$$\mathbf{W} = \begin{bmatrix} a & -b \\ c & -d \end{bmatrix},$$

where $a, b, c, d \in \mathbb{R}_{\geq 0}$. The existence of oscillations (which coincide with limit cycles in this 2D system) can be analytically characterized as follows.

Theorem 8

(Oscillations in Excitatory-Inhibitory Pairs [99]): Consider an excitatory-inhibitory pair governed by the linear-threshold dynamics (3). All network trajectories (except those with an initial condition at an unstable equilibrium) converge to a limit

cycle if and only if

$$d+2<a, \tag{20a}$$
$$(a-1)(d+1)<bc, \tag{20b}$$
$$(a-1)m_1<bm_2, \tag{20c}$$
$$0<u_1<bm_2-(a-1)m_1, \tag{20d}$$
$$0<(d+1)u_1-bu_2<[bc-(a-1)(d+1)]m_1. \tag{20e}$$

The conditions for limit cycles in E-I pairs in Theorem 8 correspond to when the system has no stable equilibria and have simple biological intuitions. Equation (20a) requires the positive feedback among the neurons of the excitatory population to be sufficiently stronger than the negative feedback among the inhibitory population. This, together with the strong mutual coupling (20b) between the two populations, ensures local instability of the equilibrium point in the linear regime and prevents the oscillations from damping. On the other hand, condition (20c) ensures that the upper bound on the inhibitory input to the excitatory population is high enough to balance the strong self-excitation. Finally, the conditions (20d) and (20e) require that the external inputs to the two nodes are neither excessively low nor excessively high, as it would keep the respective nodes in negative or positive saturation, respectively, which would reduce the effective dimensionality of the network to less than two and make oscillations impossible.

These necessary and sufficient conditions for limit cycles in E-I pairs are the basis for the analysis of the spreading of synchronous oscillations throughout a network of interconnected pairs in upcoming sections. We note that conditions for oscillations have also been characterized for linear-threshold networks with a variety of other structures, a discussion of which can be found in "Oscillatory Behavior in the Brain" below. In the following we discuss the spreading of oscillations in relation to epileptic seizures utilizing E-I pairs and Theorem 8. The exact characterization of oscillations in E-I pairs allows for a more complete analysis of the interconnected networks than if we instead used more general topologies.

Spreading Oscillations and Large-Scale Synchrony

As generalized seizures occur with synchronous oscillations across multiple brain regions [100], we wish to understand parameters such that oscillations occur in interconnected networks as defined by (19). While Theorem 8 provides conditions such that we have oscillations in a single region, in an interconnected network, even if these conditions are satisfied for each pair, the nodes in that region may no longer oscillate. Conversely, it could also be the case that that a node that in an individual network would not be oscillating may oscillate in the interconnected network. For instance, Figure 13 shows a network of two E-I pairs governed by the linear-threshold dynamics with synaptic weight matrices and controls

$$\mathbf{W}_1=\begin{bmatrix}4&-6\\5&-1\end{bmatrix}\quad \mathbf{W}_2=\begin{bmatrix}5&-8\\3&-2\end{bmatrix}\quad \mathbf{u}_1=\begin{bmatrix}1\\-1\end{bmatrix}\quad \mathbf{u}_2=\begin{bmatrix}1\\0\end{bmatrix},$$

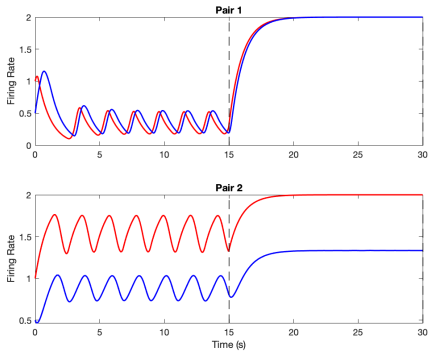

FIGURE 13 Illustration of oscillations stopping in a network following the interconnection of E-I pairs. Here the excitatory nodes are denoted by red lines and the inhibitory nodes by blue lines. Both pairs satisfy the conditions of Theorem 8 and independently oscillate, but at $t=15$ when the pairs are connected, the oscillatory behavior ends in the entire network.

with a threshold value of $\mathbf{m}=2$. Both of these networks individually satisfy the conditions of Theorem 8 and oscillate per se, see the first 15s in the plots of Figure 13. However, after interconnecting them via their excitatory nodes with interconnection matrices

$$\mathbf{W}_{12}=\mathbf{W}_{21}=\begin{bmatrix}3&0\\0&0\end{bmatrix},$$

the oscillations in the network stop, as displayed in the last 15s in the plots of Figure 13.

Figure 14 illustrates the opposite phenomena, whereby upon the interconnection of excitatory-inhibitory pairs, nodes that were not oscillating can begin to oscillate. Here we consider a network composed of three pairs, defined by the following synaptic weight matrices and controls

$$\mathbf{W}_1=\begin{bmatrix}4&-6\\5&-1\end{bmatrix}\quad \mathbf{W}_2=\begin{bmatrix}1&-5\\4&-2\end{bmatrix}\quad \mathbf{W}_3=\begin{bmatrix}3&-4\\3&-2\end{bmatrix}$$
$$\mathbf{u}_1=\begin{bmatrix}2\\-2\end{bmatrix}\quad \mathbf{u}_2=\begin{bmatrix}0\\0\end{bmatrix}\quad \mathbf{u}_3=\begin{bmatrix}0\\-1\end{bmatrix},$$

and a threshold value of 2. The first pair, governed by $\mathbf{W}_1$ oscillates on its own as per the conditions of Theorem 8, while the other two do not. In Figure 14 we show first the unconnected networks, before connecting pairs 1 and 2 and finish by connecting pair 3 to the network using the following interconnection matrices, where $\mathbf{W}_{ij}$ defines the connections from pair j to pair i.

$$\mathbf{W}_{12}=\begin{bmatrix}2&0\\0&0\end{bmatrix}\quad \mathbf{W}_{21}=\begin{bmatrix}2&0\\0&0\end{bmatrix}\quad \mathbf{W}_{13}=\begin{bmatrix}2&0\\0&-1\end{bmatrix}$$
$$\mathbf{W}_{31}=\begin{bmatrix}2&0\\0&0\end{bmatrix}\quad \mathbf{W}_{23}=\begin{bmatrix}0&0\\0&0\end{bmatrix}\quad \mathbf{W}_{32}=\begin{bmatrix}2&0\\0&0\end{bmatrix}$$

We are able to see that pair 1 maintains its oscillations throughout the interconnections, while both of the other pairs move from non-oscillating to oscillating after connecting, despite not satisfying the conditions of Theorem 8. This example illustrates the ability of the network to spread (putatively

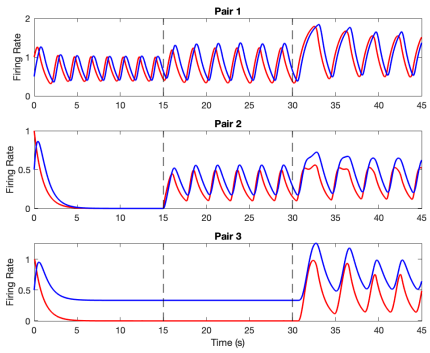

FIGURE 14 Illustration of oscillations spreading through a network of excitatory-inhibitory pairs upon interconnections. Here the excitatory nodes are denoted by red lines and the inhibitory nodes by blue lines. Initially the three pairs are distinct and only one oscillates, but as they are interconnected at $t = 15$ and $t = 30$, oscillations spread from the first pair to the others.

pathological) oscillations. We are thus interested in determining properties of the individual regions that allow for maintaining either the oscillatory or inactive behavior upon interconnection of regions. In order to do so, we condense the interconnection terms in the dynamics (19) to the following,

$$\tilde{u}_i^E(\mathbf{x}) = u_i^E + \sum_{j\neq i}(w_{ij}^{EE}x_j^E - w_{ij}^{EI}x_j^I)$$
$$\tilde{u}_i^I(\mathbf{x}) = u_i^I + \sum_{j\neq i}(w_{ij}^{IE}x_j^E - w_{ij}^{II}x_j^I). \tag{21}$$

This compiles the interconnections between the E-I pairs into one input term in the network, providing a similar form to that of an individual uncoupled E-I pair. Using this change of variables and combining it with Theorem 8, we can provide sufficient conditions for inactivity and oscillations to be maintained upon network interconnections.

Theorem 9

(Robust Behaviors in Coupled Networks [97]): Consider a network of N coupled E-I pairs defined by (19) and define the following set

$$\mathcal{U}_i = \{(u_i^E, u_i^I) \mid (20) \text{ are satisfied}\}.$$

If for all $\mathbf{x}$

$$\begin{bmatrix}\tilde{u}_i^E(\mathbf{x})\\ \tilde{u}_i^I(\mathbf{x})\end{bmatrix} \in \mathcal{U}_i,$$

then the ith pair in the network will oscillate after coupling. If, instead

$$u_i^E + \sum_{j\neq i} w_{ij}^{EE} m_j^E \leq 0,$$
$$u_i^I + \sum_{j\neq i} w_{ij}^{IE} m_j^E \leq 0,$$

the ith pair in the network does not oscillate after the network is connected.

These results provide an analytical basis for determining when E-I pairs will either be inactive or oscillate following their interconnection. By comparing this result with Theorem 8, we see that the conditions for an interconnected pair to oscillate correspond with the lack of stable equilibria of the disconnected pair when the input is replaced by the interconnected input. Some remarks are then in order. First, we note that both results are sufficient results and, as such, both the loss and spreading of oscillations can occur without them being satisfied. Second, while these results provide conditions such that oscillations or inactivity can be maintained in the event of interconnections, they do not directly provide conditions for the spreading or loss of oscillations following interconnections. In fact, they only determine if there will be no change after interconnection, rather than providing conditions on the networks such that oscillations will spread or stop. Determining direct conditions on the network parameters so that oscillations spread or disappear in a network (as shown in the prior examples) is an open problem. The work in [97] examines how the spread of oscillations throughout the network can be controlled through the modification of network weights, instead of restricting the properties of the original network itself.

These results and examples have illustrated that a network of coupled E-I pairs with the linear-threshold dynamics can exhibit a variety of oscillatory behavior. In particular, individual networks can exhibit limit cycles and, through interconnections, these oscillations can both spread throughout the network or stop altogether. As generalized seizures are related to the spread of oscillations between brain regions [96], these properties make the linear-threshold dynamics a good model for the estimation and control of this dynamical behavior.

DISCUSSION AND OPEN AVENUES

In the prior sections, we have discussed a variety of properties of the linear-threshold rate dynamics and illustrated their relevance in modeling brain behavior. This has provided an extensive look at their use in particular applications. We believe there are further dynamical properties and control mechanisms that should be studied, both in their own right, without relation to a specific brain function, as well as for exploring other avenues for using linear-threshold networks in modeling the brain. Here we provide a discussion on oscillatory properties of the dynamics with different topologies, paying special attention to the characterization of interconnections that explain observed behavior in neuronal populations, and on the potential for systems and control to inform targeted interventions that leverage the anatomical wiring structure and explain the mechanisms behind dynamic dimensionality control and spatial computing in the brain.

Oscillatory Behavior in the Brain

When observing brain networks, oscillations are omnipresent and have significant ranges in both magnitude and frequency [101]. In this work we have discussed oscillations in the context of

epileptic seizures and saw the appearance of oscillations in EEG measurements in Figure 7. However, oscillations have been linked with a large number of different cognitive tasks, such as information processing [102] and spatial cognition [103]. In our treatment of oscillations we limited the network topologies to individual and coupled E-I pairs. However, for the purposes of properly understanding the oscillatory properties of the linear-threshold dynamics and applying the model to other appearances of oscillations in the brain, it is important to consider other structures. We do this next.

Oscillations in Linear-Threshold Dynamics

In considering oscillations in linear-threshold dynamics, we recall that due to the difficulties of their exact characterization in networks of dimension greater than two, we use the proxy of lack of stable equilibria for oscillations. Indeed, using this proxy, one can show for a variety of network architectures that the linear-threshold dynamics admits oscillatory behavior of different forms, including limit cycles, quasi-periodicity, and chaos. In what follows we give a summary of oscillatory behavior in three different network architectures. We note that these network architectures do not necessarily satisfy Dale's Law, but under various assumptions can still be used as models for a brain network:

- *Competitive Networks* are characterized by having their weight matrix be a Z-matrix, which are defined by having all of their off-diagonal elements non-positive. Such networks have been studied both for the linear-threshold dynamics [104] and the unbounded threshold-linear dynamics [105]. The existence of oscillations for such networks have been classified using multiple tools: for linear-threshold dynamics, the appearance of oscillations with specific support (the set of oscillating nodes) has been shown through properties of Z-matrices and subsets of the network [104]; for threshold-linear dynamics, the lack of existence of stable equilibria is established through graph-theoretic methods [105].
- *Combinatorial Networks* are a special type of competitive network in which the weight matrix $\mathbf{W} = \{w_{ij}\}_{i,j\in\{1,\dots,n\}}$ is defined by the connections in the network and two parameters ϵ, δ as follows:

$$w_{ij} = \begin{cases} 0 & i = j, \\ -1+\epsilon & \text{if there is a connection from node } j \text{ to } i, \\ -1+\delta & \text{if there is a connection from node } j \text{ to } i, \end{cases}$$

  where $0 < \epsilon < 1$ and $\delta > 0$. Oscillations in such networks have been studied extensively for the threshold-linear dynamics [106]. In a similar fashion to the standard competitive networks, in [105] it is shown that oscillations can occur in the combinatorial threshold-linear network (CTLN), and can be constructed such that a variety of behaviors occur. Figure 15 shows that with varying network structures, limit cycles, chaos, and quasi-periodic orbits can occur. Beyond having the existence of such behavior, in [106] conditions are given that predict the number and type of both dynamic and static attractors based on analysis of sources and sinks in the graph corresponding with the network structure.
- *Coupled Networks* are those composed of a set of networks of a similar form coupled together with additional connections, such as the coupled E-I pairs (19). The oscillatory behavior of such networks can have a variety of properties. In particular, for the linear-threshold dynamics on a coupled network, in [107] three different properties of the oscillations are analyzed: regularity, synchronization, and phase-amplitude coupling. Using frequency domain techniques, a regularity index is defined with a value of 1 corresponding with no oscillations and ∞ equal to perfectly regular oscillations. As the interconnection strength increases, the regularity of the oscillations reduces and the dynamics exhibit more chaotic behavior before reaching a point which guarantees a stable equilibrium. Additionally, as the number of coupled oscillators increases, the behavior of the oscillations becomes increasingly chaotic. Figure 16 shows that, when using the Maximal Lyapunov Exponent (MLE) as a proxy for chaos, as both interconnection strength and the size of the network increases. the MLE increases until reaching the point at which stable equilibria appear and oscillations disappear. It is also shown in [107] that synchronization and phase-amplitude coupling in coupled networks increases with the interconnection strength between network components.

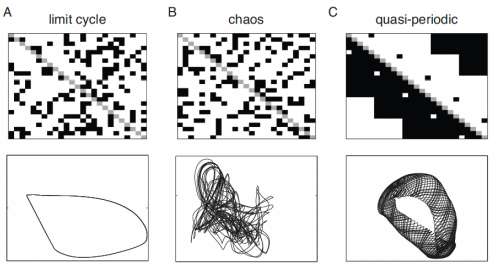

FIGURE 15 [105] Samples of the possible oscillatory behaviors with the CTLN dynamics. The top panels illustrate the pattern of the weight matrix, with black squares indicating non-zero connections, white squares indicating no connections, and diagonal self-connections in grey. The bottom panels show two-dimensional projections of the dynamics. From this we can see that under appropriate network structure and parameter choices, the CTLN dynamics exhibit a wide range of oscillatory behavior.

For further information we direct the interested reader to the above references along with [99] and the references therein.

Communication through Coherence (CTC)

We start our discussion of future avenues for the application of the linear-threshold dynamics to studying brain functions by examining communication through coherence. Communication in the brain fundamentally relies on the transmission of the

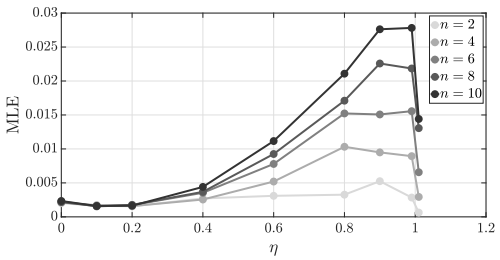

FIGURE 16 Maximal Lyapunov Exponent (MLE) as a function of network size (n) and interconnection strength between E-I pairs (η). The MLE increases as a function of both parameters until η reaches a critical value at which point the MLE drops immediately due to the lack of oscillations in the network caused by the existence of a stable equilibrium [107].

response of one neuron to the inputs arriving from another through the network [108]. When observing two brain regions, each exhibiting oscillatory behavior, that are communicating, it is common that the regions exhibit a level of synchronization. *Communication through coherence* is the idea that there exists an optimal level of synchrony, seen through the phase difference or a coherence metric, that maximizes the communication between the regions.

Due to the extensive connectivity in the brain, each region receives inputs from multiple other regions, and the CTC hypothesis provides a method to selectively process a single input at a time [109]. Within the variety of oscillatory inputs arriving, the communication from one input will exhibit a level of synchrony closer to the optimal phase difference for CTC. This input will then communicate with the brain region to a higher degree than the competing inputs and will create a response related to that stimulus. In this way, one input will be managed at a time, dictated by which input has the optimal phase difference with the activity of the region under consideration.

It has been hypothesized that the optimal phase difference for CTC is the same as the stable phase difference, that is, the phase shift that two oscillators naturally converge to in the steady state [110]. In order to numerically study CTC, it is then required to be able to compute the stable phase difference, which requires accurate knowledge of the underlying system, particularly in the case of the network generating non-sinusoidal waveforms. As accurate knowledge of the brain network is generally unavailable, which is exacerbated by the appearance of non-sinusoidal waveforms, it is desirable to be able to provide a characterization of the stable phase shift in a model-free fashion.

As a complementary avenue to existing spiking models that have been used to study CTC [109], [111], the ability of the linear-threshold network to generate oscillations, both in individual and coupled networks [107], [99], has made it an attractive option for numerically studying CTC through the determination of the stable phase shift. [110] provides a preliminary analysis of CTC using the linear-threshold dynamics through an analysis of the stable phase shift for coupled E-I oscillators. An extended study of CTC using the linear-threshold dynamics over varying network topologies and properties, however, remains an avenue for future work.

Working Memory and Spatial Computing

Working memory (WM) is a model for the short-term storage and control, in a top-down fashion, of a small number of items [112]. Representations of items can selectively be encoded into, maintained in, and deleted from WM and then manipulated for the purpose of tasks such as reasoning and decision making.

WM has been associated with oscillations in the brain and the relation between types of oscillations in different regions. In particular, WM has been suggested to rely on coupling between beta oscillations (those with a frequency between 12 and 30 Hz) and gamma oscillations (those with frequency between 30 and 100 Hz) [113]. In this model, gamma activity corresponds with spiking that encodes and maintains information in working memory, while top-down information is encoded in beta activity which inhibits gamma oscillations and thus controls access to the represented information in WM [114]. Through this, when information is being encoded into WM, the beta activity decreases and high gamma activity is observed. While information is deleted, the opposite relation appears. Note also that this interplay between beta and gamma oscillations is interestingly similar to that during selective attention, where the attentional state follows a (theta-frequency) rhythmic switch between a 'sampling' state and a 'shifting' state [115]. The sampling state involves increased beta oscillations in the frontal eye field (FEF, a motor processing area) and gamma activity in the lateral intraparietal cortex (LIP, a sensory processing area) linked to attention suppression and sensory enhancement, respectively. During the shifting state, in contrast, both oscillations are suppressed, leading to reduced visual processing before an attentional shift. Various other similarities and shared mechanisms have also been suggested between working memory (as internal attention) and (external) selective attention, see, for example, [116], [18], [117], [118]. However, as with any model, this relationship between gamma and beta waves does not fully explain the neural mechanisms underlying WM. In particular, the anti-correlated increases and decreases in gamma and beta behavior provides an 'on-off' concept for WM [114]. However, with the oscillations representing large populations of neurons, this model is unable to explain how individual item representations are manipulated. One such hypothesis for how WM encodes such information is called 'spatial computing'. In this setup, the gamma-beta interaction is used to encode representations, while the spatial movement of this activity across a cortical network is used for the purpose of manipulating the information to the relevant task [119]. The variety of oscillatory behavior illustrated by the linear-threshold dynamics provides an avenue to model the gamma-beta interactions in WM. In addition, the fact that oscillations can spread through linear-threshold networks and the availability of analytical tools to characterize when and how, provides an opportunity to quantitatively model spatial computing.

Linear-Threshold Dynamics with Network Plasticity

Throughout this work we have discussed using the linear-threshold dynamics as a model for the brain and studied properties of the dynamics for a given synaptic weight matrix. However, the brain is plastic [120], [121], [122] and the connections between neurons can both increase and decrease in magnitude, resulting in a changing synaptic weight matrix. A related, but distinct process that also occurs in the brain is neurogenesis, namely, the generation of new neurons in the brain, resulting in networks with additional (at the macroscale) or modified (at the mesoscale) nodes [123].

Both of these processes and their associated brain functions can be studied through the lens of linear-threshold dynamics with a synaptic weight matrix that is itself dynamic. One particular function related to both neuroplasticity and neurogenesis is memory [124], [125], [73], [126], [127]. We modeled declarative memory using the threshold-linear dynamics, with memories being represented by a set of nodes that permit a stable equilibrium point. With the basis for memory representation using the threshold-linear dynamics in place, this opens itself for extension to covering the concept of neuroplasticity and neurogenesis on memory. The work [73] encodes memories in 'flexible' networks, which are those where the synaptic weight matrix can be perturbed by a small amount. This correlates with the concept of neuroplasticity and investigating neurogenesis in memory models through the threshold-linear dynamics, which forms an interesting avenue for future work.

The idea of plasticity in the brain is also key to the ideas of artificial neural networks and machine learning, where the changing wiring in the brain is represented by training the weights of the synaptic weight matrix in order to perform relevant tasks. An issue that appears in machine learning is *catastrophic forgetting*, in which changing the weights result in the network forgetting how to perform previously learned tasks [128]. However, this is not a phenomenon that appears in the human brain. One proposed mechanism for how the brain avoids this issue is that the interactions between the thalamus and cortex result in specific components of the cortex being active for specific tasks [129]. This idea of specific components of the cortex being active aligns with the idea of permitted and forbidden sets that appeared in the model of memory using linear-threshold networks (as in "Declarative Memory in Single Region Linear-Threshold Rate Models"). As such, further study of thalamocortical linear-threshold networks for avoiding catastrophic forgetting in machine learning is another potential avenue for future work.

Controller Synthesis in Linear-Threshold Networks

In both the single and multi-region networks considered in this work, we consider the convergence of the dynamics to either constant equilibria or trajectories with varying forms. The convergence of the network to specific trajectories is important for a variety of problems, including goal-driven selective attention, or memory recall. However, determining conditions and control inputs such that the network converges to a specific non-zero equilibrium or trajectory is difficult. When using a hierarchical approach, the values of the trajectory are given by recursively defined signals, and choosing parameters to set these maps to specific values is unrealistic, especially for large systems. On the other hand, if considering the network as a whole, it can be difficult to fully understand stability and stabilization issues, and the choice of parameters might not be particularly robust.

Further, an issue that arises in both approaches is that frequently the synaptic weight matrix is not known, or only is known as a (potentially poor) estimate. Machine learning methods can be of use in approaching the synthesis of controllers that make the network converge to explicit trajectories. These methods can be used both to provide a model of how the brain functions internally (such as how specific signals are achieved in selective attention or memory recall), or to determine a method for external modulation of the brain to achieve desired activity (such as deep brain stimulation). One such approach that has been used in this context is reservoir computing [130], [131] due to its origins in computational neuroscience, with specific applications to linear-threshold networks considered in [86]. There are many interesting avenues for future research in the area of determining explicit signals with machine learning, such as comparing the use of different learning models and methods.

CONCLUSIONS

The development of computational models with sufficient biological realism *and* mathematical tractability is one of the key goals in computational neuroscience. In this work, we have investigated one such model at the mesoscale, the linear-threshold rate dynamics. Due to the wide array of functions the brain performs, any model of the brain that aims to cover multiple applications must exhibit a rich suite of behaviors. Through discussions of a variety of behaviors exhibited by the brain, we have shown the linear-threshold dynamics to be a rich and versatile model.

Through modeling of GDSA in both single and interconnected networks of different topologies, we showed the linear-threshold dynamics are stabilizable through simultaneous selective inhibition of task-irrelevant nodes and selective recruitment of task-relevant ones. Using a model of declarative memory as sets of neurons that can be the support sets of stable equilibria, we illustrated that the unbounded version of the linear-threshold dynamics can permit multiple stable equilibrium points and is conditionally multiattractive. In addition, we illustrated that the dynamics admit both bifurcations and oscillatory behavior in E-I pairs, two dynamical properties that occur during epileptic seizures.

We finished by extending the discussion of oscillations beyond the E-I pair network structure and discussing additional dynamical brain processes such as communication through coherence and spatial computing. While this is neither a comprehensive list of all properties of the linear-threshold dynamics nor a complete collection of brain functions it could be used on, this

work highlights the rich behavior of this family of mesoscopic models, illustrates its significant utility in modeling brain activity, and showcases the benefits of adopting a perspective from systems and controls to analyze how neuronal networks optimize their computational capabilities. We hope our exposition will spur further investigations at the intersection of neuroscience and control to realize the potential of network and control-theoretic tools in deepening our understanding of the interplay between structure and dynamics in the brain, its role in shaping dynamical behavior, performance, and robustness, and the mechanisms that govern information transfer.

ACKNOWLEDGMENT

This work was supported by NSF CMMI-2308639 and MURI ARO W911NF-24-1-0228.

AUTHOR INFORMATION

Michael McCreesh received the B.A.Sc and M.A.Sc degrees in Mathematics and Engineering from Queen's University, Kingston, Canada in 2017 and 2019, resp. He received the Ph.D. degree in Mechanical Engineering from the University of California San Diego in 2024. His current research interests include control theory and its application to theoretical neuroscience, in particular the application of dynamical systems to model brain networks.

Erfan Nozari is an Assistant Professor at the University of California, Riverside Department of Mechanical Engineering. He received the B.Sc. degree in Electrical Engineering-Control in 2013 from Isfahan University of Technology, Iran, and the Ph.D. in Mechanical Engineering and Cognitive Science in 2019 from University of California San Diego. He was subsequently a postdoctoral researcher at the University of Pennsylvania Department of Electrical and Systems Engineering. His main research interests lie at the intersection of computational neuroscience, dynamical systems, and machine learning and his lab's recent focus has been on understanding the neural code and its generative mechanisms across spatial and temporal scales using the unique perspective of dynamical systems and controls. He is a Hellman Fellow and has been the recipient of the NSF CAREER Award, the IEEE Transactions on Control of Network Systems Outstanding Paper Award, and Best Student Paper Awards from the IEEE Conference on Decision and Control and the American Control Conference.

Jorge Cortés (M'02, SM'06, F'14) received the Licenciatura degree in mathematics from Universidad de Zaragoza, Zaragoza, Spain, in 1997, and the Ph.D. degree in engineering mathematics from Universidad Carlos III de Madrid, Madrid, Spain, in 2001. He held postdoctoral positions with the University of Twente, Twente, The Netherlands, and the University of Illinois at Urbana-Champaign, Urbana, IL, USA. He was an Assistant Professor with the Department of Applied Mathematics and Statistics, University of California, Santa Cruz, CA, USA, from 2004 to 2007. He is currently a Professor and Cymer Corporation Endowed Chair in High Performance Dynamic Systems Modeling and Control at the Department of Mechanical and Aerospace Engineering, University of California, San Diego, CA, USA. He is a Fellow of IEEE, SIAM, and IFAC. His current research interests include distributed control and optimization, network science, nonsmooth analysis, reasoning and decision making under uncertainty, network neuroscience, and multi-agent coordination in robotic, power, and transportation networks.

REFERENCES

[1] S. J. Schiff, *Neural Control Engineering: the Emerging Intersection between Control Theory and Neuroscience*. Cambridge, MA: MIT Press, 2012.

[2] S. Ching, M. Y. Liberman, J. J. Chemali, M. B. Westover, J. D. Kenny, K. Solt, P. L. Purdon, and E. N. Brown, "Real-time closed-loop control in a rodent model of medically induced coma using burst suppression," *Anesthesiology: The Journal of the American Society of Anesthesiologists*, vol. 119, no. 4, pp. 848–860, 2013.

[3] S. Gu, F. Pasqualetti, M. Cieslak, Q. K. Telesford, A. B. Yu, A. E. Kahn, J. D. Medaglia, J. M. Vettel, M. B. Miller, S. T. Grafton, and D. S. Bassett, "Controllability of structural brain networks," *Nature Communications*, vol. 6, p. 8414, October 2015.

[4] S. V. Sarma and P. Sacré, "Characterizing complex human behaviors and neural responses using dynamic models," in *Dynamic Neuroscience: Statistics, Modeling, and Control* (Z. Chen and S. V. Sarma, eds.), pp. 177–195, Springer, 2018.

[5] M. S. Madhav and N. J. Cowan, "The synergy between neuroscience and control theory: the nervous system as inspiration for hard control challenges," *Annual Review of Control, Robotics, and Autonomous Systems*, vol. 3, pp. 243–267, 2020.

[6] E. Nozari and J. Cortés, "Hierarchical selective recruitment in linear-threshold brain networks. Part I: Intra-layer dynamics and selective inhibition," *IEEE Transactions on Automatic Control*, vol. 66, no. 3, pp. 949–964, 2021.

[7] E. Nozari and J. Cortés, "Hierarchical selective recruitment in linear-threshold brain networks. Part II: Inter-layer dynamics and top-down recruitment," *IEEE Transactions on Automatic Control*, vol. 66, no. 3, pp. 965–980, 2021.

[8] P. Srivastava, E. Nozari, J. Z. Kim, H. Ju, D. Zhou, C. Becker, F. Pasqualetti, G. J. Pappas, and D. S. Bassett, "Models of communication and control for brain networks: distinctions, convergence, and future outlook," *Network Neuroscience*, vol. 4, no. 4, pp. 1122–1159, 2020.

[9] G. Drion, T. O'Leary, J. Dethier, A. Franci, and R. Sepulchre, "Neuronal behaviors: a control perspective," in *IEEE Conf. on Decision and Control*, (Osaka, Japan), Dec. 2015. Tutorial.

[10] M. E. Broucke, "Adaptive internal model theory of the oculomotor system and the cerebellum," *IEEE Transactions on Automatic Control*, vol. 66, no. 11, pp. 5444–5450, 2021.

[11] M. E. Broucke, "Adaptive internal models in neuroscience," *Foundations and Trends in Systems and Control*, vol. 9, no. 4, pp. 365–550, 2022.

[12] C. A. Coté, "A dynamic systems theory model of visual perception development," *Journal of Occupational Therapy, Schools, & Early Intervention*, vol. 8, no. 2, pp. 157–169, 2015.

[13] A. Kukona and W. Tabor, "Impulse processing: A dynamical systems model of incremental eye movements in the visual world paradigm," *Cognitive Science*, vol. 35, no. 6, pp. 1009–1051, 2011.

[14] M. Kawato, K. Furukawa, and R. Suzuki, "A hierarchical neural-network model for control and learning of voluntary movement," *Biological Cybernetics*, vol. 57, pp. 169–185, 1987.

[15] K. V. Shenoy, M. T. Kaufman, M. Sahani, and M. M. Churchland, "A dynamical systems view of motor preparation: implications for neural prosthetic system design," *Progress in Brain Research*, vol. 192, pp. 33–58, 2011.

[16] C. I. Connolly, J. B. Burns, and M. S. Jog, "A dynamical-systems model for Parkinson's disease," *Biological Cybernetics*, vol. 83, pp. 47–59, 2000.

[17] E. J. Müller, S. J. van Albada, J. W. Kim, and P. A. Robinson, "Unified neural field theory of brain dynamics underlying oscillations in Parkinson's disease and generalized epilepsies," *Journal of Theoretical Biology*, vol. 428, pp. 132–146, 2017.

[18] A. Gazzaley and A. C. Nobre, "Top-down modulation: bridging selective attention and working memory," *Trends in Cognitive Sciences*, vol. 16, no. 2, pp. 129–135, 2012.

[19] R. Quentin, J. King, E. Sallard, N. Fishman, R. Thompson, E. R. Buch, and

L. G. Cohen, "Differential brain mechanisms of selection and maintenance of information during working memory," *Journal of Neuroscience*, vol. 39, no. 19, pp. 3728–3740, 2019.

[20] G. L. Holmes, "Cognitive impairment in epilepsy: the role of network abnormalities," *Epileptic Disorders*, vol. 17, no. 2, pp. 101–116, 2015.

[21] Y. Höller and E. Trinka, "Is there a relation between EEG-slow waves and memory dysfunction in epilepsy? a critical appraisal," *Frontiers in Human Neuroscience*, vol. 9, p. 341, 2015.

[22] C. R. Butler and A. Z. Zeman, "Recent insights into the impairment of memory in epilepsy: transient epileptic amnesia, accelerated long-term forgetting and remote memory impairment," *Brain*, vol. 131, no. 9, pp. 2243–2263, 2008.

[23] A. L. Hodgkin and A. F. Huxley, "A quantitative description of membrane current and its application to conduction and excitation in nerve," *The Journal of Physiology*, vol. 117, no. 4, pp. 500–544, 1952.

[24] G. B. Ermentrout and D. H. Terman, *Mathematical Foundations of Neuroscience*, vol. 35. New York: Springer, 2010.

[25] E. M. Izhikevich, *Dynamical Systems in Neuroscience*. Cambridge, MA: MIT Press, 2007.

[26] P. Dayan and L. F. Abbott, *Theoretical Neuroscience: Computational and Mathematical Modeling of Neural Systems*. Computational Neuroscience, Cambridge, MA: MIT Press, 2001.

[27] E. Nozari, M. A. Bertolero, J. Stiso, L. Caciagli, E. J. Cornblath, X. He, A. S. Mahadevan, G. J. Pappas, and D. S. Bassett, "Macroscopic resting-state brain dynamics are best described by linear models," *Nature Biomedical Engineering*, vol. 8, no. 1, pp. 68–84, 2024.

[28] M. Breakspear, "Dynamic models of large-scale brain activity," *Nature Neuroscience*, vol. 20, no. 3, pp. 340–352, 2017.

[29] X. Li, D. Coyle, L. Maguire, T. M. McGinnity, and H. Benali, "A model selection method for nonlinear system identification based fMRI effective connectivity analysis," *IEEE Transactions on Medical Imaging*, vol. 30, no. 7, pp. 1365–1380, 2011.

[30] K. E. Stephan, L. Kasper, L. M. Harrison, J. Daunizeau, H. E. M. den Ouden, M. Breakspear, and K. J. Friston, "Nonlinear dynamic causal models for fMRI," *Neuroimage*, vol. 42, no. 2, pp. 649–662, 2008.

[31] S. Ahmed and E. Nozari, "On the linearizing effect of spatial averaging in large-scale populations of homogeneous nonlinear systems," in *IEEE Conf. on Decision and Control*, (Cancun, Mexico), pp. 641–648, Dec. 2022.

[32] G. T. Einevoll, C. Kayser, N. K. Logothetis, and S. Panzeri, "Modelling and analysis of local field potentials for studying the function of cortical circuits," *Nature Reviews Neuroscience*, vol. 14, no. 11, pp. 770–785, 2013.

[33] S. Keeley, Á. Byrne, A. Fenton, and J. Rinzel, "Firing rate models for gamma oscillations," *Journal of Neurophysiology*, vol. 121, no. 6, pp. 2181–2190, 2019.

[34] T. Schwalger and A. V. Chizhov, "Mind the last spike — firing rate models for mesoscopic populations of spiking neurons," *Current Opinion in Neurobiology*, vol. 58, pp. 155–166, 2019.

[35] J. Feng and K. P. Hadeler, "Qualitative behaviour of some simple networks," *Journal of Physics A: Mathematical and General*, vol. 29, no. 16, pp. 5019–5033, 1996.

[36] P. C. Bressloff, "Spatiotemporal dynamics of continuum neural fields," *Journal of Physics A: Mathematical and Theoretical*, vol. 45, no. 3, p. 033001, 2011.

[37] K. D. Miller and F. Fumarola, "Mathematical equivalence of two common forms of firing rate models of neural networks," *Neural Computation*, vol. 24, no. 1, pp. 25–31, 2012.

[38] V. Centorrino, A. Gokhale, A. Davydov, G. Russo, and F. Bullo, "Euclidean contractivity of neural networks with symmetric weights," *IEEE Control Systems Letters*, vol. 7, pp. 1724–1729, 2023.

[39] Q. Liu, A. Ulloa, and B. Horwitz, "Using a large-scale neural model of cortical object processing to investigate the neural substrate for managing multiple items in short-term memory," *Journal of Cognitive Neuroscience*, vol. 29, no. 11, pp. 1860–1876, 2017.

[40] M. Kajiwara, R. Nomura, F. Goetze, M. Kawabata, Y. Isomura, T. Akutsu, and M. Shimono, "Inhibitory neurons exhibit high controlling ability in the cortical microconnectome," *PLOS Computational Biology*, vol. 17, no. 4, p. e1008846, 2021.

[41] J. Chen, U. Hasson, and C. Honey, "Processing timescales as an organizing principle for primate cortex," *Neuron*, vol. 88, no. 2, pp. 244–246, 2015.

[42] M. Bear, B. Connors, and M. A. Paradiso, *Neuroscience: Exploring the Brain*. Jones & Bartlett Learning, 2020.

[43] S. M. Sherman and R. W. Guillery, *Exploring the Thalamus and Its Role in Cortical Function*. Cambridge, MA: MIT Press, 2006.

[44] S. J. Kiebel, J. Daunizeau, and K. J. Friston, "A hierarchy of time-scales and the brain," *PLOS Computational Biology*, vol. 4, no. 11, p. e1000209, 2008.

[45] K. George and J. M. Das, "Neuroanatomy, thalamocortical radiations," *StatPearls [Internet]*, 2020.

[46] S. M. Sherman, "Thalamocortical interactions," *Current Opinion in Neurobiology*, vol. 22, no. 4, pp. 575–579, 2012.

[47] L. Gabernet, S. P. Jadhav, D. E. Feldman, M. Carandini, and M. Scanziani, "Somatosensory integration controlled by dynamic thalamocortical feed-forward inhibition," *Neuron*, vol. 48, no. 2, pp. 315–327, 2005.

[48] S. Cruikshank, T. J. Lewis, and B. Connors, "Synaptic basis for intense thalamocortical activation of feedforward inhibitory cells in neocortex," *Nature Neuroscience*, vol. 10, no. 4, pp. 462–468, 2007.

[49] K. Delevich, J. Tucciarone, Z. J. Huang, and B. Li, "The mediodorsal thalamus drives feedforward inhibition in the anterior cingulate cortex via parvalbumin interneurons," *Journal of Neuroscience*, vol. 35, no. 14, pp. 5743–5753, 2015.

[50] J. T. Porter, C. K. Johnson, and A. Agmon, "Diverse types of interneurons generate thalamus-evoked feedforward inhibition in the mouse barrel cortex," *Journal of Neuroscience*, vol. 21, no. 8, pp. 2699–2710, 2001.

[51] H. A. Swadlow, "Thalamocortical control of feed-forward inhibition in awake somatosensory 'barrel'cortex," *Philosophical Transactions of the Royal Society of London. Series B: Biological Sciences*, vol. 357, no. 1428, pp. 1717–1727, 2002.

[52] E. K. Kosmidis and J. Vibert, "Feed-forward inhibition in the visual thalamus," *Neurocomputing*, vol. 44, pp. 479–487, 2002.

[53] J. S. Isaacson and M. Scanziani, "How inhibition shapes cortical activity," *Neuron*, vol. 72, no. 2, pp. 231–243, 2011.

[54] R. Desimone and J. Duncan, "Neural mechanisms of selective visual attention," *Annual Review of Neuroscience*, vol. 18, no. 1, pp. 193–222, 1995.

[55] J. Moran and R. Desimone, "Selective attention gates visual processing in the extrastriate cortex," *Science*, vol. 229, no. 4715, pp. 782–784, 1985.

[56] B. C. Motter, "Focal attention produces spatially selective processing in visual cortical areas V1, V2, and V4 in the presence of competing stimuli," *Journal of Neurophysiology*, vol. 70, no. 3, pp. 909–919, 1993.

[57] N. Lavie, "Distracted and confused?: Selective attention under load," *Trends in Cognitive Sciences*, vol. 9, no. 2, pp. 75–82, 2005.

[58] P. Foldiak, "Sparse coding in the primate cortex," in *The Handbook of Brain Theory and Neural Networks* (M. A. Arbib, ed.), pp. 1064–1068, Cambridge, MA: MIT Press, 2nd ed., 2003.

[59] M. Imani, A. Rahimi, D. Kong, T. Rosing, and J. M. Rabaey, "Exploring hyperdimensional associative memory," in *IEEE International Symposium on High Performance Computer Architecture*, (Austin, TX), pp. 445–456, 2017.

[60] F. L. D. Silva, W. Blanes, S. N. Kalitzin, J. Parra, P. Suffczynski, and D. N. Velis, "Epilepsies as dynamical diseases of brain systems: basic models of the transition between normal and epileptic activity," *Epilepsia*, vol. 44, pp. 72–83, 2003.

[61] R. A. Stefanescu, R. G. Shivakeshavan, and S. S. Talathi, "Computational models of epilepsy," *Seizure*, vol. 21, no. 10, pp. 748–759, 2012.

[62] C. J. Stam, "Nonlinear dynamical analysis of EEG and MEG: review of an emerging field," *Clinical Neurophysiology*, vol. 116, no. 10, pp. 2266–2301, 2005.

[63] E. Niedermeyer and F. H. L. da Silva, *Electroencephalography: Basic Principles, Clinical Applications, and Related Fields*. Lippincott Williams & Wilkins, 2005.

[64] J. Touboul, F. Wendling, P. Chauvel, and O. Faugeras, "Neural mass activity, bifurcations, and epilepsy," *Neural Computation*, vol. 23, no. 12, pp. 3232–3286, 2011.

[65] F. Celi, A. Allibhoy, F. Pasqualetti, and J. Cortés, "Linear-threshold dynamics for the study of epileptic events," *IEEE Control Systems Letters*, vol. 5, no. 4, pp. 1405–1410, 2021.

[66] E. M. Izhikevich, "Neural excitability, spiking and bursting," *International Journal of Bifurcation and Chaos*, vol. 10, no. 06, pp. 1171–1266, 2000.

[67] W. T. Blume, "Focal and generalized: both here and there," *Epilepsy Currents*, vol. 10, no. 5, pp. 115–117, 2010.

[68] J. W. Bang, J. Choi, and K. R. Park, "Noise reduction in brainwaves by using both EEG signals and frontal viewing camera images," *Sensors*, vol. 13, no. 5, pp. 6272–6294, 2013.

[69] A. Baddeley, "Working memory," in *Memory*, pp. 71–111, Routledge, 2020.

[70] J. J. Hopfield, "Neural networks and physical systems with emergent collective computational abilities," *Proceedings of the National Academy of Sciences*, vol. 79, no. 8, pp. 2554–2558, 1982.

[71] G. E. Hinton and T. J. Sejnowski, "Learning and relearning in Boltzmann machines," in *Parallel Distributed Processing: Explorations in the Microstructure of Cognition: Foundations* (D. E. Rumelhart, J. L. McClelland, and the PDP Research Group, eds.), vol. 1, pp. 282–317, Cambridge, MA: MIT Press, 1986.

[72] R. H. R. Hahnloser, H. S. Seung, and J. J. Slotine, "Permitted and forbidden sets in symmetric threshold-linear networks," *Neural Computation*, vol. 15, no. 3, pp. 621–638, 2003.

[73] C. Curto, A. Degeratu, and V. Itskov, "Flexible memory networks," *Bulletin of Mathematical Biology*, vol. 74, no. 3, pp. 590–614, 2012.

[74] K. M. Tye, E. K. Miller, F. H. Taschbach, M. K. Benna, M. Rigotti, and S. Fusi, "Mixed selectivity: Cellular computations for complexity," *Neuron*, vol. 112, no. 14, pp. 2289–2303, 2024.

[75] M. Rigotti, O. Barak, M. R. Warden, X. Wang, N. D. Daw, E. K. Miller, and S. Fusi, "The importance of mixed selectivity in complex cognitive tasks," *Nature*, vol. 497, no. 7451, pp. 585–590, 2013.

[76] A. S. Mitchell, "The mediodorsal thalamus as a higher order thalamic relay nucleus important for learning and decision-making," *Neuroscience & Biobehavioral Reviews*, vol. 54, pp. 76–88, 2015.

[77] E. J. Ramcharan, J. W. Gnadt, and S. M. Sherman, "Higher-order thalamic relays burst more than first-order relays," *Proceedings of the National Academy of Sciences*, vol. 102, no. 34, pp. 12236–12241, 2005.

[78] M. C. Schmid, S. W. Mrowka, J. Turchi, R. C. Saunders, M. Wilke, A. J. Peters, F. Q. Ye, and D. A. Leopold, "Blindsight depends on the lateral geniculate nucleus," *Nature*, vol. 466, no. 7304, pp. 373–377, 2010.

[79] N. Tinbergen, "The hierarchical organization of nervous mechanisms underlying instinctive behaviour," in *Symposium for the Society for Experimental Biology*, vol. 4, pp. 305–312, 1950.

[80] A. R. Luria, "The functional organization of the brain," *Scientific American*, vol. 222, no. 3, pp. 66–79, 1970.

[81] D. Meunier, R. Lambiotte, A. Fornito, K. Ersche, and E. T. Bullmore, "Hierarchical modularity in human brain functional networks," *Frontiers in Neuroinformatics*, vol. 3, p. 37, 2009.

[82] B. Gauthier, E. Eger, G. Hesselmann, A. Giraud, and A. Kleinschmidt, "Temporal tuning properties along the human ventral visual stream," *Journal of Neuroscience*, vol. 32, no. 41, pp. 14433–14441, 2012.

[83] U. Hasson, J. Chen, and C. J. Honey, "Hierarchical process memory: memory as an integral component of information processing," *Trends in Cognitive Sciences*, vol. 19, no. 6, pp. 304–313, 2015.

[84] J. A. Harris, S. Mihalas, K. E. Hirokawa, J. D. Whitesell, H. Choi, A. Bernard, P. Bohn, S. Caldejon, L. Casal, A. Cho, A. Feiner, D. Feng, N. Gaudreault, C. R. Gerfen, N. Graddis, P. A. Groblewski, A. M. Henry, A. Ho, R. Howard, J. E. Knox, L. Kuan, X. Kuang, J. Lecoq, P. Lesnar, Y. Li, J. Luviano, S. McConoughey, M. T. Mortrud, M. Naeemi, L. Ng, S. W. Oh, B. Oullette, E. Shen, S. A. Sorenson, W. Wakeman, Q. Wang, Y. Wang, A. Williford, J. W. Phillips, A. R. Jones, C. Koch, and H. Zeng, "Hierarchical organization of cortical and thalamic connectivity," *Nature*, vol. 575, no. 7781, pp. 195–202, 2019.

[85] M. McCreesh and J. Cortés, "Selective inhibition and recruitment in linear-threshold thalamocortical networks," *IEEE Transactions on Control of Network Systems*, vol. 11, no. 1, pp. 375–388, 2024.

[86] M. McCreesh and J. Cortés, "Control of linear-threshold brain networks via reservoir computing," *IEEE Open Journal of Control Systems*, vol. 3, pp. 325–341, 2024.

[87] V. Veliov, "A generalization of the Tikhonov theorem for singularly perturbed differential inclusions," *Journal of Dynamical & Control Systems*, vol. 3, no. 3, pp. 291–319, 1997.

[88] A. A. Moustafa, R. D. McMullan, B. Rostron, D. H. Hewedi, and H. H. Haladjian, "The thalamus as a relay station and gatekeeper: relevance to brain disorders," *Reviews in the Neurosciences*, vol. 28, no. 2, pp. 203–218, 2017.

[89] R. W. Guillery and S. M. Sherman, "Thalamic relay functions and their role in corticocortical communication: generalizations from the visual system," *Neuron*, vol. 33, no. 2, pp. 163–175, 2002.

[90] K. E. Chu, "Generalization of the Bauer-Fike theorem," *Numerische Mathematik*, vol. 49, no. 6, pp. 685–691, 1986.

[91] G. K. Kostopoulos, "Involvement of the thalamocortical system in epileptic loss of consciousness," *Epilepsia*, vol. 42, pp. 13–19, 2001.

[92] R. D. Traub, "Fast oscillations and epilepsy," *Epilepsy Currents*, vol. 3, no. 3, pp. 77–79, 2003.

[93] P. Chauvel, "Stereo-electroencephalography," *Multimethodological Assessment of the Epileptic Forms*, pp. 135–163, 1996.

[94] O. Devinsky, A. Vezzani, T. J. O'Brien, N. Jette, I. E. Scheffer, M. de Curtis, and P. Perucca, "Epilepsy (primer)," *Nature Reviews: Disease Primers*, vol. 4, no. 1, 2018.

[95] S. Spencer, "Neural networks in human epilepsy: evidence of and implications for treatment," *Epilepsia*, vol. 43, no. 3, pp. 219–227, 2002.

[96] M. Stead, M. Bower, B. Brinkmann, K. Lee, W. Marsh, F. Meyer, B. Litt, J. V. Gompel, and G. Worrell, "Microseizures and the spatiotemporal scales of human partial epilepsy," *Brain*, vol. 133, no. 9, pp. 2789–2797, 2010.

[97] A. Allibhoy, F. Celi, F. Pasqualetti, and J. Cortés, "Optimal network interventions to control the spreading of oscillations," *IEEE Open Journal of Control Systems*, vol. 1, pp. 141–151, 2022.

[98] E. A. Coddington and N. Levinson, *Theory of Ordinary Differential Equations*. New York: McGraw-Hill, 1955.

[99] E. Nozari, R. Planas, and J. Cortés, "Structural characterization of oscillations in brain networks with rate dynamics," *Automatica*, vol. 146, p. 110653, 2022.

[100] L. G. Dominguez, R. A. Wennberg, W. Gaetz, D. Cheyne, O. C. Snead, and J. L. P. Velazquez, "Enhanced synchrony in epileptiform activity? local versus distant phase synchronization in generalized seizures," *Journal of Neuroscience*, vol. 25, no. 35, pp. 8077–8084, 2005.

[101] G. Buzsaki, *Rhythms of the Brain*. Oxford, UK: Oxford University Press, 2006.

[102] C. Beste, A. Münchau, and C. Frings, "Towards a systematization of brain oscillatory activity in actions," *Communications Biology*, vol. 6, no. 1, p. 137, 2023.

[103] J. B. Caplan, J. R. Madsen, S. Raghavachari, and M. J. Kahana, "Distinct patterns of brain oscillations underlie two basic parameters of human maze learning," *Journal of Neurophysiology*, vol. 86, no. 1, pp. 368–380, 2001.

[104] M. McCreesh, T. Menara, and J. Cortés, "Sufficient conditions for oscillations in competitive linear-threshold brain networks," *IEEE Control Systems Letters*, vol. 7, pp. 2886–2891, 2023.

[105] K. Morrison, A. Degeratu, V. Itskov, and C. Curto, "Diversity of emergent dynamics in competitive threshold-linear networks," *SIAM Journal on Applied Dynamical Systems*, vol. 23, no. 1, pp. 855–884, 2024.

[106] C. Parmelee, S. Moore, K. Morrison, and C. Curto, "Core motifs predict dynamic attractors in combinatorial threshold-linear networks," *PloS One*, vol. 17, no. 3, p. e0264456, 2022.

[107] E. Nozari and J. Cortés, "Oscillations and coupling in interconnections of two-dimensional brain networks," in *American Control Conference*, (Philadelphia, PA), pp. 193–198, July 2019.

[108] P. Fries, "Rhythms for cognition: Communication through coherence," *Neuron*, vol. 88, pp. 220–235, 2015.

[109] D. McLelland and R. VanRullen, "Theta-gamma coding meets communication-through-coherence: neuronal oscillatory multiplexing theories reconciled," *PLOS Computational Biology*, vol. 12, no. 10, p. e1005162, 2016.

[110] E. Nozari and J. Cortés, "Communication through coherence: Analysis of the optimal phase shift and the importance of waveform shape," in *Neuroscience*, (Chicago, IL), Oct. 2019. Poster.

[111] D. Reyner-Parra and G. Huguet, "Phase-locking patterns underlying effective communication in exact firing rate models of neural networks," *PLOS Computational Biology*, vol. 18, no. 5, p. e1009342, 2022.

[112] A. H. V. Lautz, J. Herding, S. Ludwig, T. Nierhaus, B. Maess, A. Villringer, and F. Blankenburg, "Gamma and beta oscillations in human MEG encode the contents of vibrotactile working memory," *Frontiers in Human Neuroscience*, vol. 11, p. 576, 2017.

[113] E. K. Miller, M. Lundqvist, and A. M. Bastos, "Working memory 2.0," *Neuron*, vol. 100, no. 2, pp. 463–475, 2018.

[114] M. Lundqvist, P. Herman, M. R. Warden, S. L. Brincat, and E. K. Miller, "Gamma and beta bursts during working memory readout suggest roles in its volitional control," *Nature Communications*, vol. 9, no. 1, p. 394, 2018.

[115] I. C. Fiebelkorn and S. Kastner, "A rhythmic theory of attention," *Trends in Cognitive Sciences*, vol. 23, no. 2, pp. 87–101, 2019.

[116] E. Awh and J. Jonides, "Overlapping mechanisms of attention and spatial working memory," *Trends in Cognitive Sciences*, vol. 5, no. 3, pp. 119–126, 2001.

[117] A. Kiyonaga and T. Egner, "Working memory as internal attention: Toward

an integrative account of internal and external selection processes," *Psychonomic Bulletin & Review*, vol. 20, pp. 228–242, 2013.

[118] N. E. Myers, M. G. Stokes, and A. C. Nobre, "Prioritizing information during working memory: beyond sustained internal attention," *Trends in Cognitive Sciences*, vol. 21, no. 6, pp. 449–461, 2017.

[119] M. Lundqvist, S. L. Brincat, J. Rose, M. W. Warden, T. J. Buschman, E. K. Miller, and P. Herman, "Working memory control dynamics follow principles of spatial computing," *Nature Communications*, vol. 14, no. 1, p. 1429, 2023.

[120] B. Kolb and R. Gibb, "Brain plasticity and behaviour in the developing brain," *Journal of the Canadian Academy of Child and Adolescent Psychiatry*, vol. 20, no. 4, p. 265, 2011.

[121] P. Mateos-Aparicio and A. Rodríguez-Moreno, "The impact of studying brain plasticity," *Frontiers in Cellular Neuroscience*, vol. 13, p. 66, 2019.

[122] J. Lisman and N. Spruston, "Postsynaptic depolarization requirements for LTP and LTD: a critique of spike timing-dependent plasticity," *Nature Neuroscience*, vol. 8, no. 7, pp. 839–841, 2005.

[123] A. Kumar, V. Pareek, M. A. Faiq, S. K. Ghosh, and C. Kumari, "Adult neurogenesis in humans: a review of basic concepts, history, current research, and clinical implications," *Innovations in Clinical Neuroscience*, vol. 16, no. 5-6, p. 30, 2019.

[124] D. N. Abrous and J. M. Wojtowicz, "Interaction between neurogenesis and hippocampal memory system: new vistas," *Cold Spring Harbor Perspectives in Biology*, vol. 7, no. 6, p. a018952, 2015.

[125] W. Deng, J. B. Aimone, and F. H. Gage, "New neurons and new memories: how does adult hippocampal neurogenesis affect learning and memory?," *Nature Reviews Neuroscience*, vol. 11, no. 5, pp. 339–350, 2010.

[126] R. C. Cassilhas, S. Tufik, and M. T. de Mello, "Physical exercise, neuroplasticity, spatial learning and memory," *Cellular and Molecular Life Sciences*, vol. 73, pp. 975–983, 2016.

[127] M. Fisher, C. Holland, M. M. Merzenich, and S. Vinogradov, "Using neuroplasticity-based auditory training to improve verbal memory in schizophrenia," *American Journal of Psychiatry*, vol. 166, no. 7, pp. 805–811, 2009.

[128] R. M. French, "Catastrophic forgetting in connectionist networks," *Trends in Cognitive Sciences*, vol. 3, no. 4, pp. 128–135, 1999.

[129] M. B. Wang and M. M. Halassa, "Thalamocortical contribution to flexible learning in neural systems," *Network Neuroscience*, vol. 6, no. 4, pp. 980–997, 2022.

[130] J. Z. Kim and D. S. Bassett, "A neural machine code and programming framework for the reservoir computer," *Nature Machine Intelligence*, vol. 5, no. 6, pp. 622–630, 2023.

[131] F. Damicelli, C. C. Hilgetag, and A. Goulas, "Brain connectivity meets reservoir computing," *PLoS Computational Biology*, vol. 18, no. 11, p. e1010639, 2022.

[132] D. A. Henze, Z. Borhegyi, J. Csicsvari, M. A. Mamiya, K. D. Harris, and G. Buzsaki, "Intracellular features predicted by extracellular recordings in the hippocampus in vivo," *Journal of Neurophysiology*, vol. 84, no. 1, pp. 390–400, 2000.

[133] D. A. Henze, K. D. Harris, Z. Borhegyi, J. Csicsvari, A. Mamiya, H. Hirase, A. Sirota, and G. Buzsaki, "Simultaneous intracellular and extracellular recordings from hippocampus region ca1 of anesthetized rats." CRCNS.org, 2009.

[134] N. T. Carnevale and M. L. Hines, *The NEURON book*. Cambridge, UK: Cambridge University Press, 2006.

[135] S. O. Burns, D. Xing, and R. M. Shapley, "Comparisons of the dynamics of local field potential and multiunit activity signals in macaque visual cortex," *Journal of Neuroscience*, vol. 30, no. 41, pp. 13739–13749, 2010.

[136] T. Heiberg, B. Kriener, T. Tetzlaff, G. T. Einevoll, and H. E. Plesser, "Firing-rate models for neurons with a broad repertoire of spiking behaviors," *Journal of Computational Neuroscience*, vol. 45, pp. 103–132, 2018.

[137] C. Curto, A. Degeratu, and V. Itskov, "Encoding binary neural codes in networks of threshold-linear neurons," *Neural Computation*, vol. 25, no. 11, pp. 2858–2903, 2013.

[138] J. Sully, "The psycho-physical process in attention," *Brain*, vol. 13, no. 2, pp. 145–164, 1890.

[139] A. M. Treisman, "Strategies and models of selective attention.," *Psychological Review*, vol. 76, no. 3, p. 282, 1969.

[140] E. C. Cherry, "Some experiments on the recognition of speech, with one and with two ears," *The Journal of the Acoustical Society of America*, vol. 25, no. 5, pp. 975–979, 1953.

[141] L. Itti and C. Koch, "Computational modelling of visual attention," *Nature Reviews Neuroscience*, vol. 2, no. 3, p. 194, 2001.

[142] M. A. Pinsk, G. M. Doniger, and S. Kastner, "Push-pull mechanism of selective attention in human extrastriate cortex," *Journal of Neurophysiology*, vol. 92, no. 1, pp. 622–629, 2004.

[143] K. Tóth, K. T. Hofer, A. Kandrács, L. Entz, A. Bagó, L. Erőss, Z. Jordán, G. Nagy, A. Sólyom, D. Fabó, I. Ulbert, and L. Wittner, "Hyperexcitability of the network contributes to synchronization processes in the human epileptic neocortex," *The Journal of Physiology*, vol. 596, no. 2, pp. 317–342, 2018.

[144] H. G. E. Meijer, T. L. Eissa, B. Kiewiet, J. F. Neuman, C. A. Schevon, R. G. Emerson, R. R. Goodman, G. M. M. Jr., C. J. Marcuccilli, A. K. Tryba, J. D. Cowan, S. A. van Gils, and W. van Drongelen, "Modeling focal epileptic activity in the Wilson-Cowan model with depolarization block," *Journal of Mathematical Neuroscience*, vol. 5, pp. 1–17, 2015.

[145] A. Coletti, "On Jansen-Rit system modeling epilepsy phenomena," in *International Conference on New Trends in the Applications of Differential Equations in Sciences*, pp. 281–292, Springer, 2022.

[146] V. K. Jirsa, W. C. Stacey, P. P. Quilichini, A. I. Ivanov, and C. Bernard, "On the nature of seizure dynamics," *Brain*, vol. 137, no. 8, pp. 2210–2230, 2014.

[147] D. Sritharan and S. V. Sarma, "Fragility in dynamic networks: application to neural networks in the epileptic cortex," *Neural Computation*, vol. 26, no. 10, pp. 2294–2327, 2014.

[148] D. Ehrens, D. Sritharan, and S. V. Sarma, "Closed-loop control of a fragile network: application to seizure-like dynamics of an epilepsy model," *Frontiers in Neuroscience*, vol. 9, p. 58, 2015.

[149] E. T. Wang, M. Vannucci, Z. Haneef, R. Moss, V. R. Rao, and S. Chiang, "A Bayesian switching linear dynamical system for estimating seizure chronotypes," *Proceedings of the National Academy of Sciences*, vol. 119, no. 46, p. e2200822119, 2022.

[150] W. James, *The Principles of Psychology*, vol. 1. Cosimo, Inc., 1890.

[151] G. Miller, "Human memory and the storage of information," *IRE Transactions on Information Theory*, vol. 2, no. 3, pp. 129–137, 1956.

[152] R. C. Atkinson and R. M. Shiffrin, "Human memory: A proposed system and its control processes," in *Psychology of Learning and Motivation*, vol. 2, pp. 89–195, Elsevier, 1968.

[153] G. R. Loftus and E. F. Loftus, *Human Memory: The Processing of Information*. Psychology Press, 1st ed., 1976.

[154] D. L. Schacter and E. Tulving, "What are the memory systems of 1994?," *Memory Systems*, vol. 1994, p. 424, 1994.

[155] S. Ganguli, D. Huh, and H. Sompolinsky, "Memory traces in dynamical systems," *Proceedings of the National Academy of Sciences*, vol. 105, no. 48, pp. 18970–18975, 2008.

[156] R. Pascanu and H. Jaeger, "A neurodynamical model for working memory," *Neural Networks*, vol. 24, no. 2, pp. 199–207, 2011.

[157] S. Albeverio, A. Khrennikov, and P. E. Kloeden, "Memory retrieval as a p-adic dynamical system," *Biosystems*, vol. 49, no. 2, pp. 105–115, 1999.

[158] I. Tsuda, E. Koerner, and H. Shimizu, "Memory dynamics in asynchronous neural networks," *Progress of Theoretical Physics*, vol. 78, no. 1, pp. 51–71, 1987.

[159] M. Wolff and S. D. Vann, "The cognitive thalamus as a gateway to mental representations," *Journal of Neuroscience*, vol. 39, no. 1, pp. 3–14, 2019.

[160] H. Gudden, "Klinische und anatomische beiträge zur kenntniss der multiplen alkoholneuritis nebst bemerkungen über die regenerationsvorgänge im peripheren nervensystem," *Archiv für Psychiatrie und Nervenkrankheiten*, vol. 28, no. 3, pp. 643–741, 1896.

[161] E. Ahissar and T. Oram, "Thalamic relay or cortico-thalamic processing? Old question, new answers," *Cerebral Cortex*, vol. 25, no. 4, pp. 845–848, 2015.

[162] Y. B. Saalmann and S. Kastner, "Cognitive and perceptual functions of the visual thalamus," *Neuron*, vol. 71, no. 2, pp. 209–223, 2011.

[163] S. M. Sherman and R. W. Guillery, "Functional organization of thalamocortical relays," *Journal of Neurophysiology*, vol. 76, no. 3, pp. 1367–1395, 1996.

[164] A. S. Mitchell, S. M. Sherman, M. A. Sommer, R. G. Mair, R. P. Vertes, and Y. Chudasama, "Advances in understanding mechanisms of thalamic relays in cognition and behavior," *Journal of Neuroscience*, vol. 34, no. 46, pp. 15340–15346, 2014.

[165] F. Alcaraz, V. Fresno, A. R. Marchand, E. J. Kremer, E. Coutureau, and M. Wolff, "Thalamocortical and corticothalamic pathways differentially contribute to goal-directed behaviors in the rat," *Elife*, vol. 7, p. e32517, 2018.

[166] L. Logiaco, L. F. Abbott, and S. Escola, "Thalamic control of cortical dynamics

in a model of flexible motor sequencing," *Cell Reports*, vol. 35, no. 9, 2021.

[167] J. M. Alonso and H. A. Swadlow, "Thalamus controls recurrent cortical dynamics," *Nature Neuroscience*, vol. 18, no. 12, pp. 1703–1704, 2015.

[168] M. M. Halassa and L. Acsády, "Thalamic inhibition: diverse sources, diverse scales," *Trends in Neurosciences*, vol. 39, no. 10, pp. 680–693, 2016.

[169] S. R. Cole and B. Voytek, "Brain oscillations and the importance of waveform shape," *Trends in Cognitive Sciences*, vol. 21, no. 2, pp. 137–149, 2017.

[170] G. Buzsáki and A. Draguhn, "Neuronal oscillations in cortical networks," *Science*, vol. 304, no. 5679, pp. 1926–1929, 2004.

[171] L. V. Gambuzza, A. Cardillo, A. Fiasconaro, L. Fortuna, J. Gómez-Gardenes, and M. Frasca, "Analysis of remote synchronization in complex networks," *Chaos: An Interdisciplinary Journal of Nonlinear Science*, vol. 23, no. 4, p. 043103, 2013.

[172] H. Sakaguchi and Y. Kuramoto, "A soluble active rotater model showing phase transitions via mutual entertainment," *Progress of Theoretical Physics*, vol. 76, no. 3, pp. 576–581, 1986.

[173] Y. Qin, *Distributed coordination and partial synchronization in complex networks*. PhD thesis, University of Groningen, 2019.

[174] V. Vuksanović and P. Hövel, "Functional connectivity of distant cortical regions: role of remote synchronization and symmetry in interactions," *NeuroImage*, vol. 97, pp. 1–8, 2014.

[175] L. Gollo, C. Mirasso, and A. Villa, "Dynamic control for synchronization of separated cortical areas through thalamic relay," *NeuroImage*, vol. 52, no. 3, pp. 947–955, 2010.

[176] V. Nicosia, M. Valencia, M. Chavez, A. Díaz-Guilera, and V. Latora, "Remote synchronization reveals network symmetries and functional modules," *Physical Review Letters*, vol. 110, no. 17, p. 174102, 2013.